

# **Ab initio calculations on SnCl<sub>2</sub> and Franck-Condon factor simulations of its $\tilde{a}$ - $\tilde{X}$ and $\tilde{B}$ - $\tilde{X}$ absorption and single-vibronic-level emission spectra**

Edmond P. F. Lee<sup>a)</sup>

Department of Building Services Engineering, the Hong Kong Polytechnic University,  
Hung Hom, Hong Kong

John M. Dyke

School of Chemistry, University of Southampton, Highfield, Southampton SO17 1BJ, United Kingdom

Daniel K. W. Mok<sup>b),c)</sup>

Department of Applied Biology and Chemical Technology, the Hong Kong Polytechnic University,  
Hung Hom, Hong Kong

Wan-ki Chow<sup>b),d)</sup>

Department of Building Services Engineering, the Hong Kong Polytechnic University,  
Hung Hom, Hong Kong

Foo-tim Chau

Department of Applied Biology and Chemical Technology, the Hong Kong Polytechnic University,  
Hung Hom, Hong Kong

(Received 16 March 2007; accepted 22 May 2007; published online 13 July 2007)

Minimum-energy geometries, harmonic vibrational frequencies, and relative electronic energies of some low-lying singlet and triplet electronic states of stannous dichloride, SnCl<sub>2</sub>, have been computed employing the complete-active-space self-consistent-field/multireference configuration interaction (CASSCF/MRCI) and/or restricted-spin coupled-cluster single-double plus perturbative triple excitations [RCCSD(T)] methods. The small core relativistic effective core potential, ECP28MDF, was used for Sn in these calculations, together with valence basis sets of up to augmented correlation-consistent polarized-valence quintuple-zeta (aug-cc-pV5Z) quality. Effects of outer core electron correlation on computed geometrical parameters have been investigated, and contributions of off-diagonal spin-orbit interaction to relative electronic energies have been calculated. In addition, RCCSD(T) or CASSCF/MRCI potential energy functions of the  $\tilde{X}^1A_1$ ,  $\tilde{a}^3B_1$ , and  $\tilde{B}^1B_1$  states of SnCl<sub>2</sub> have been computed and used to calculate anharmonic vibrational wave functions of these three electronic states. Franck-Condon factors between the  $\tilde{X}^1A_1$  state, and the  $\tilde{a}^3B_1$  and  $\tilde{B}^1B_1$  states of SnCl<sub>2</sub>, which include anharmonicity and Duschinsky rotation, were then computed, and used to simulate the  $\tilde{a}$ - $\tilde{X}$  and  $\tilde{B}$ - $\tilde{X}$  absorption and corresponding single-vibronic-level emission spectra of SnCl<sub>2</sub> which are yet to be recorded. It is anticipated that these simulated spectra will assist spectroscopic identification of gaseous SnCl<sub>2</sub> in the laboratory and/or will be valuable in *in situ* monitoring of SnCl<sub>2</sub> in the chemical vapor deposition of SnO<sub>2</sub> thin films in the semiconductor gas sensor industry by laser induced fluorescence and/or ultraviolet absorption spectroscopy, when a chloride-containing tin compound, such as tin dichloride or dimethyldichlorotin, is used as the tin precursor. © 2007 American Institute of Physics. [DOI: 10.1063/1.2749508]

## INTRODUCTION

Stannous [tin(II)] dichloride, SnCl<sub>2</sub>, is of importance in a variety of industrial applications. For example, in the polymer industry, Si/SnCl<sub>2</sub> has been established to be an environmentally friendly and efficient silicone-inorganic fire retardant.<sup>1-3</sup> Various other catalytic and/or synergic roles of

SnCl<sub>2</sub> have also been demonstrated recently on numerous occasions, such as, in the palladium-catalyzed cyclocarbonylation of monoterpenes,<sup>4</sup> the PdCl<sub>2</sub>/SnCl<sub>2</sub> electrodeless deposition of copper on micronic NiTi shape memory alloy particles,<sup>5</sup> the mild, ecofriendly and fast reductions of nitroarenes to aminoarenes using stannous dichloride dihydrate in ionic liquid tetrabutylammonium bromide,<sup>6</sup> and the SnCl<sub>2</sub>-mediated carbonyl allylation reaction between aldehydes and allyl halides in fully aqueous media.<sup>7</sup> More relevant to the present study, however, is the role of SnCl<sub>2</sub> in the semiconductor gas sensor industry<sup>8-10</sup> specifically in the process of chemical vapor deposition (CVD).<sup>11,12</sup> For instance, SnO<sub>2</sub> thin films with uniform thickness or fine par-

<sup>a)</sup>Also at Department of Applied Biology and Chemical Technology, the Hong Kong Polytechnic University and School of Chemistry, University of Southampton.

<sup>b)</sup>Authors to whom correspondence should be addressed.

<sup>c)</sup>Electronic mail: bedaniel@polyu.edu.hk

<sup>d)</sup>Electronic mail: bewkchow@polyu.edu.hk

ticles with uniform size used in gas sensors are often produced in high temperature gas-phase processes, e.g., CVD, high-temperature flow reactors, and flames. Normally, chlorides and organotin compounds, such as tin dichloride, tin tetrachloride, tetramethyltin, and dimethyldichlorotin, are used as Sn precursors for the gas-phase synthesis.<sup>11–13</sup> SnCl<sub>2</sub>, either as a precursor or an intermediate in the oxidation reaction leading to SnO<sub>2</sub> in the CVD process, is present near the surface layer of the growing SnO<sub>2</sub> thin film. In order to achieve efficient process control of an industrial high yield/high volume CVD reactor, *in situ* monitoring of gaseous species, including SnCl<sub>2</sub>, in the CVD reactor under different experimental conditions by a spectroscopic technique is often carried out.<sup>12,14,15</sup> This would yield valuable information on the reaction mechanism involved in the CVD process. Recently, both Fourier transform infrared spectroscopy and near infrared tunable diode laser spectroscopy have been employed for this purpose in the CVD of SnO<sub>2</sub> thin films.<sup>9,12</sup> Nevertheless, several other spectroscopic techniques, including laser induced fluorescence (LIF) spectroscopy<sup>16–19</sup> and ultraviolet absorption spectroscopy,<sup>20–23</sup> have been used routinely to measure the densities of reactive intermediates in processing-type plasmas, such as in flame, laser, hot filament, and plasma enhanced CVD processes in the semiconductor industry.<sup>24–29</sup> Prior to *in situ* monitoring of gaseous species in a CVD reactor, the spectroscopic technique of LIF followed by dispersed fluorescence [single-vibronic-level (SVL) emission] has been employed extensively in the laboratory to characterize the reactive gas-phase species<sup>30–37</sup> to be monitored in the CVD process. In this connection, we propose in the present study to carry out a combined *ab initio*/Franck-Condon factor investigation on the absorption and SVL emission spectra of SnCl<sub>2</sub>, yet to be recorded. Our ongoing, combined *ab initio*/Franck-Condon factor computational research program has investigated the LIF,<sup>38,39</sup> SVL emission<sup>40–43</sup> absorption,<sup>15</sup> chemiluminescence,<sup>43,44</sup> photoelectron,<sup>45–48</sup> and photodetachment<sup>49,50</sup> spectra of a number of triatomic species. It has been shown that, combining state-of-the-art *ab initio* calculations with Franck-Condon (FC) factor calculations including anharmonicity, highly reliable simulated electronic spectra with vibrational structure can be produced, and in this way, significant contributions to the analyses of corresponding experimental spectra have been made. In a number of cases, our computed FC factors and/or spectral simulations have led to revisions of previous spectral assignments, including establishing the molecular carrier and/or electronic states involved in the electronic transition, and/or assignments of the observed vibrational structure.<sup>41,44,47,50</sup> These studies demonstrate the predictive power of our combined *ab initio*/FC computational technique, and hence, it is believed that simulated spectra thus produced in the present study will facilitate future *in situ* monitoring of gaseous SnCl<sub>2</sub> molecules in a CVD process by LIF and/or ultraviolet absorption spectroscopy. At the same time, it is hoped that the present study would stimulate spectroscopists to record the LIF, absorption, and/or dispersed fluorescence spectra of SnCl<sub>2</sub>. The present study is also a continuation of similar previous studies by us on the

dihalides of some lighter group 14 (IV-A) elements, namely, CF<sub>2</sub>,<sup>15,49,51</sup> CCl<sub>2</sub>,<sup>50</sup> SiCl<sub>2</sub>,<sup>40</sup> and GeCl<sub>2</sub>.<sup>38</sup>

In fact, SnCl<sub>2</sub> has received considerable attention from spectroscopists<sup>52–63</sup> and computational chemists.<sup>64–72</sup> Previous spectroscopic studies include Raman,<sup>54,58</sup> electron diffraction,<sup>55–57</sup> emission,<sup>52,53</sup> and photoelectron studies.<sup>59–63</sup> However, although the geometrical parameters and vibrational frequencies of the  $\tilde{X}^1A_1$  state of SnCl<sub>2</sub> have been derived and/or measured from previous spectroscopic studies (*infra vide*), the only experimental information available on the excited states of SnCl<sub>2</sub> has come from two emission studies, which published emission spectra of SnCl<sub>2</sub> recorded from a discharge<sup>52</sup> and from flames<sup>53</sup> over 40 years ago. The agreement between the reported experimental  $T_0$  values of 22 237 (Ref. 52) and 22 249 (Ref. 53) cm<sup>-1</sup> (i.e., 2.757 and 2.759 eV, respectively) and available computed multireference configuration interaction (MRCI) and coupled-cluster single-double plus perturbative triple excitations [CCSD(T)]  $T_e$  values of 2.61 (Ref. 65) and 2.68 (Ref. 67) eV, respectively, obtained for the  $\tilde{a}^3B_1$  state of SnCl<sub>2</sub> can be considered as only modest (*infra vide*). Moreover, the only reported experimental vibrational frequencies of 240 and 80 cm<sup>-1</sup> tentatively assigned to  $\nu'_1$  and  $\nu'_2$  of the upper state of SnCl<sub>2</sub> in the emission spectrum<sup>53</sup> do not agree well with the only available computed harmonic vibrational frequencies of 336 and 136 cm<sup>-1</sup> obtained for the symmetric stretching and bending modes, respectively, of the  $\tilde{a}^3B_1$  state of SnCl<sub>2</sub> from density functional theory (DFT) calculations.<sup>66</sup> (Although Ref. 66 quotes computed  $\omega_1$ ,  $\omega_2$ , and  $\omega_3$  values of 370, 58, and 382 cm<sup>-1</sup> for the  $\tilde{a}^3B_1$  state of SnCl<sub>2</sub> from CI calculations of Ref. 64, we are unable to trace these values from the original reference. We speculate that there are some typing errors in Table III of Ref. 66 and these values are most likely from DFT calculations of Ref. 66; *infra vide*.) In fact, the only excited state, other than the (1)<sup>3</sup>B<sub>1</sub> state, which has been investigated by *ab initio* calculations, is the (1)<sup>1</sup>B<sub>1</sub> state.<sup>65</sup> Clearly, further and more reliable calculations on low-lying excited states of SnCl<sub>2</sub> are required in order to confirm or revise the assignments of the available emission spectra.<sup>52,53</sup>

Lastly, the lowest singlet-triplet gaps of the dihalides of the group 14 elements have recently been receiving considerable attention (see, for example, Ref. 50 and references therein), as also shown in some recent DFT and *ab initio* investigations on SnCl<sub>2</sub>.<sup>65–67</sup> It should also be noted that our previously reported, simulated  $\tilde{a}^3B_1$ - $\tilde{X}^1A_1$  and  $\tilde{A}^1B_1$ - $\tilde{X}^1A_1$  absorption spectra of GeCl<sub>2</sub> agree reasonably well with the corresponding experimental LIF spectra, especially for the  $\tilde{a}$ - $\tilde{X}$  band system (see Ref. 38 and reference therein). In addition, very recently, a further LIF study on the  $\tilde{A}$ - $\tilde{X}$  band system of GeCl<sub>2</sub>, with previously unreported dispersed fluorescence spectra of this band system, has been published,<sup>31</sup> and also a computational study on GeCl<sub>2</sub> dimer, which attempts to explain the congested region of the  $\tilde{A}$ - $\tilde{X}$  LIF band system of GeCl<sub>2</sub>, has appeared.<sup>73</sup> These very recent spectroscopic and computational studies on GeCl<sub>2</sub> show the continued interest in this group of very important reactive intermediates of dihalides of the group 14 elements.

TABLE I. Basis sets used for Sn and Cl.

Basis	Sn				Cl		
	ECP <sup>a</sup>	Augmented <sup>b</sup>	Frozen <sup>c</sup>	Correlated <sup>d</sup>	All electrons	Frozen <sup>e</sup>	Nb <sup>f</sup>
A	AVQZ		4s4p4d	5s <sup>2</sup> 5p <sup>2</sup>	AV(Q+d)Z <sup>g</sup>	1s2s2p	270
A <sub>So</sub>	AVQZ <sup>h</sup>		4s4p4d	5s <sup>2</sup> 5p <sup>2</sup>	AV(Q+d)Z <sup>h</sup>	1s2s2p	272
A <sub>f</sub>	AVQZ <sup>i</sup>		4s4p4d	5s <sup>2</sup> 5p <sup>2</sup>	AV(Q+d)Z <sup>i</sup>	1s2s2p	216
A1	AVQZ	2d1f1g	4s4p	4d <sup>10</sup> 5s <sup>2</sup> 5p <sup>2</sup>	AV(Q+d)Z <sup>g</sup>	1s2s2p	296
A2	AVQZ	3s2p2d1f1g		4s <sup>2</sup> 4p <sup>6</sup> 4d <sup>10</sup> 5s <sup>2</sup> 5p <sup>2</sup>	AV(Q+d)Z <sup>g</sup>	1s2s2p	305
A3	AVQZ	3s2p2d1f1g		4s <sup>2</sup> 4p <sup>6</sup> 4d <sup>10</sup> 5s <sup>2</sup> 5p <sup>2</sup>	ACVQZ <sup>j</sup>	1s	395
B	AV5Z		4s4p4d	5s <sup>2</sup> 5p <sup>3</sup>	AV(5+d)Z <sup>g</sup>	1s2s2p	411
B1	AV5Z	2d1f1g1h	4s4p	4d <sup>10</sup> 5s <sup>2</sup> 5p <sup>3</sup>	AV(5+d)Z <sup>g</sup>	1s2s2p	448
B2	AV5Z	2s2p2d1f1g1h		4s <sup>2</sup> 4p <sup>6</sup> 4d <sup>10</sup> 5s <sup>2</sup> 5p <sup>3</sup>	AV(5+d)Z <sup>g</sup>	1s2s2p	456

<sup>a</sup>The ECP28MDF ECP (Ref. 76) was used with the corresponding standard ECP28MDF<sub>aug-cc-pVQZ</sub> (AVQZ) or ECP28MDF<sub>aug-cc-pV5Z</sub> (AV5Z) valence basis sets (Refs. 77–79).

<sup>b</sup>The augmented uncontracted functions given are for outer core electrons of Sn, when they are correlated in the RCCSD(T) calculations. For the AVQZ basis set, the augmented functions have the following exponents: 3s(9.0,3.6,1.44), 2p(2.5,1.0), 2d(2.5,1.0), 1f(1.4), and 1g(1.4). For the AV5Z basis set, the augmented functions are 2s(3.5,1.7), 2p(3.2,1.6), 2d(3.875,1.55), 1f(1.3), 1g(1.3), and 1h(1.2).

<sup>c</sup>Each of these shells of Sn is accounted for by a single contracted function in the standard ECP basis sets. They are frozen in the correlation calculations.

<sup>d</sup>These Sn electrons are correlated (with augmented appropriate sets of tight functions; see footnote b).

<sup>e</sup>These shells of Cl are frozen in the correlation calculations.

<sup>f</sup>Total numbers of contracted Gaussian functions in the basis sets used for SnCl<sub>2</sub>.

<sup>g</sup>The standard all-electron aug-cc-pV(Q+d)Z {AV(Q+d)} or aug-cc-pV(5+d)Z {AV(5+d)} basis sets were used for Cl (Ref. 80).

<sup>h</sup>Uncontracted s, p, and d functions of the standard basis sets were used in CASSCF spin-orbit interaction calculations; see text.

<sup>i</sup>The g functions in both the basis sets of Sn and Cl are excluded in the survey CASSCF calculations; see Table III.

<sup>j</sup>The standard aug-cc-pwCVQZ basis set was used for Cl (Refs. 79 and 80).

## THEORETICAL CONSIDERATIONS AND COMPUTATIONAL DETAILS

### Ab initio calculations

The basis sets, frozen cores, and correlated electrons employed in the calculations are summarized in Table I. The computational strategy is described as follows: Firstly, the single-reference restricted-spin couple-cluster single-double plus perturbative triple excitations [RCCSD(T)] method<sup>74</sup> was employed primarily for calculations on the closed-shell singlet  $\tilde{X}^1A_1$  state and low-lying high-spin triplet excited states of SnCl<sub>2</sub>. For low-lying, low-spin, open-shell singlet states, which cannot be described adequately by a single-configuration wave function, the multireference complete-active-space self-consistent field/multireference configuration interaction (CASSCF/MRCI) method<sup>75</sup> was used. Nevertheless, some CASSCF/MRCI calculations were also performed on the  $\tilde{X}^1A_1$  and  $\tilde{a}^3B_1$  states of SnCl<sub>2</sub>, for the purposes of evaluating the relative electronic energies of some low-lying open-shell singlet states (with respect to the  $\tilde{X}^1A_1$  state) and also assessing the reliability of the CASSCF/MRCI method [compared to the RCCSD(T) method; *infra vide*]. In general, the active space employed in the CASSCF/MRCI calculation is a full valence active space, plus the appropriate outer core electrons if required (see Table I), unless otherwise stated (*infra vide*). The largest CI configuration space used in the MRCI calculations performed in the present study is that for the  $\tilde{a}^3B_1$  state at the CASSCF/MRCI/A1 level, i.e., it includes Sn 4d<sup>10</sup> electrons in the active space, and it consists of  $\sim 95.9 \times 10^6$  contracted configurations and  $65.8 \times 10^9$  uncontracted configurations in the MRCI calculations. Lastly, it should be noted that in the geometry optimization of the open-shell singlet states, the

computed (MRCI+D) energy (i.e., MRCI energy plus the Davidson correction) was optimized.

Secondly, regarding the basis sets used, the fully relativistic effective core potential, ECP28MDF,<sup>76,77</sup> which accounts for scalar relativistic effects, has been used for Sn. Standard basis sets<sup>78,79</sup> of augmented correlation-consistent valence-polarized quadruple-zeta (aug-cc-pVQZ; denoted A in Table I and the following text) and quintuple-zeta (aug-cc-pV5Z; denoted B) qualities have been used for both Sn and Cl [note that the aug-cc-pV(X+d)Z basis sets, X=Q or 5, i.e., with an extra tight d set, were used for Cl;<sup>80</sup> see Table I]. In addition, different outer core electrons of Sn and/or Cl were included successively in the correlation treatment with extra appropriate sets of tight functions designed based on standard basis sets A and B (basis sets A1, A2, and A3 of QZ quality and B1 and B2 of 5Z quality; see Table I, and footnotes for the exponents of the extra tight functions designed for the outer core). Contributions from core correlation of different levels (i.e., including different core electrons in the correlation calculation) and extrapolation to the complete basis set (CBS) limit can be estimated based on the series of calculations carried out using different basis sets and/or including different core electrons as given in Table I (*infra vide*).

Finally, since the ground and low-lying excited electronic states of SnCl<sub>2</sub> have C<sub>2v</sub> structures (see next section), and are therefore nondegenerate states, they do not have diagonal spin-orbit splittings. Nevertheless, off-diagonal spin-orbit interactions between states, which are close to each other in energy, could be significant for a molecule containing the heavy fourth row element Sn. Consequently, CASSCF spin-orbit interaction calculations were carried out at the RCCSD(T)/A optimized geometry of the  $\tilde{X}^1A_1$  state of

TABLE II. The ranges of bond lengths [ $r(\text{SnCl})$  in Å] and bond angles [ $\theta(\text{ClSnCl})$  in °], and the number of points of the RCCSD(T)/B and CASSCF/MRCI/A energy scans, which were used for the fitting of the potential energy functions (PEFs) of the  $\tilde{X}^1A_1$ ,  $\tilde{a}^3B_1$ , and  $\tilde{B}^1B_1$  states of  $\text{SnCl}_2$ , and the maximum vibrational quantum numbers of the symmetric stretching ( $\nu_1$ ) and bending ( $\nu_2$ ) modes of the harmonic basis used in the variational calculations of the anharmonic vibrational wave functions of each electronic state and the restrictions of the maximum values of  $(\nu_1 + \nu_2)$ ; see text, and Refs. 42 and 45 for details.

Energy scans	$\tilde{X}^1A_1$	$\tilde{a}^3B_1$	$\tilde{B}^1B_1$
Range of $r$	$1.77 \leq r \leq 3.50$	$1.74 \leq r \leq 3.28$	$1.88 \leq r \leq 2.94$
Range of $\theta$	$65.0 \leq \theta \leq 150.0$	$64.0 \leq \theta \leq 159.0$	$73.0 \leq \theta \leq 167.0$
Points	130	110	97
Max. $\nu_1$	8	8	8
Max. $\nu_2$	30	30	30
Max. $(\nu_1 + \nu_2)$	30	30	30
Method	RCCSD(T)/B	RCCSD(T)/B	CASSCF/MRCI+D/A

$\text{SnCl}_2$  in order to assess spin-orbit contributions to the computed vertical excitation energies. Nine states, namely, the lowest singlet and triplet states of each symmetry of the  $C_{2v}$  point group and also the  $(2)^1A_1$  states, were considered in the average-state CASSCF spin-orbit calculations. The spin-orbit pseudopotential of the ECP28MDF ECP for Sn, uncontracted  $s$ ,  $p$ , and  $d$  functions of basis set A ( $A_{\text{so}}$  in Table I), and the computed CASSCF/MRCI+D/A (MRCI energies including the Davidson correction) energies for the spin-orbit diagonal elements were employed. For the  $^3B_2$  state, the relative computed MRCI+D/A energy obtained employing a larger active space than the full valence active space was used (*infra vide*). For the  $(2)^1A_1$  state, the relative computed MRCI+D/A energy obtained in the two state [i.e.,  $(1)^1A_1$  and  $(2)^1A_1$  states] CASSCF/MRCI calculations was used (*infra vide*). The effects of spin-orbit interaction on the computed relative energies were largely found to be small. (While the  $\tilde{X}^1A_1$  state of  $\text{SnCl}_2$  was lowered in energy by 0.003 eV by spin-orbit interaction, all the excited states considered were raised by less than 0.006 eV; computed spin-orbit splittings in all the triplet states considered are less than 0.003 eV.) Consequently, it has been decided to ignore spin-orbit contributions in the energy scans for the fitting of the potential energy functions (PEFs) to be described in the next subsection.

All *ab initio* calculations carried out in the present study have employed the MOLPRO suite of programs.<sup>81</sup>

## POTENTIAL ENERGY FUNCTIONS, ANHARMONIC VIBRATIONAL WAVE FUNCTIONS, AND FRANCK-CONDON FACTOR CALCULATIONS

The details of the coordinates and polynomial employed for the potential energy function, the rovibrational Hamiltonian<sup>82</sup> and anharmonic vibrational wave functions used in the variational calculations, and the FC factor calculations including Duschinsky rotation have been described previously<sup>38,42,45,49</sup> and hence will not be repeated here. Some technical details specific to the present study are, however, summarized in Table II, including the ranges of bond lengths [ $r(\text{SnCl})$  in angstroms] and bond angles [ $\theta(\text{ClSnCl})$  in degrees], and the number of points in the RCCSD(T)/B or

CASSCF/MRCI/A energy scans, which were used for the fitting of the PEFs of the  $\tilde{X}^1A_1$ ,  $\tilde{a}^3B_1$ , and  $\tilde{B}^1B_1$  states of  $\text{SnCl}_2$ , and the maximum vibrational quantum numbers of the symmetric stretching ( $\nu_1$ ) and bending ( $\nu_2$ ) modes of the harmonic basis used in the variational calculations of the anharmonic vibrational wave functions of each electronic state and the restrictions of the maximum values of  $(\nu_1 + \nu_2)$ .

It should be noted firstly that, although it has been found in the present study that the first excited singlet state of  $\text{SnCl}_2$  is the  $\tilde{A}^1A_2$  state (*infra vide*), this state has neither been considered for FC factor calculations nor spectral simulations. There are three reasons for this decision. First, the electronic transition between the  $\tilde{X}^1A_1$  and  $\tilde{A}^1A_2$  state is dipole forbidden. It should, however, be noted that vibronic coupling involving the asymmetric stretching vibrational mode of  $b_2$  symmetry can lead to nonadiabatic interaction between the  $\tilde{A}^1A_2$  and  $\tilde{B}^1B_1$  states, although this consideration is beyond the scope of the present study. The second reason for ignoring the  $\tilde{A}^1A_2$  state in this part of our investigation is that the equilibrium bond angle,  $\theta_e$ , of the  $\tilde{A}^1A_2$  state is computed in the range of  $\sim 61^\circ - 67^\circ$ , which is considerably smaller than the equilibrium bond angle of the  $\tilde{X}^1A_1$  state (by over  $30^\circ$ ; *infra vide*). Consequently, the FC factors in the vertical excitation region between these two states are expected to be very small. Finally, the observed emission, absorption, and/or LIF spectra of dichlorides of the lighter members of the group 14 elements have been assigned to transition(s) between the  $(1)^3B_1$  (and/or  $(1)^1B_1$  state(s), and the  $\tilde{X}^1A_1$  state (see Refs. 31, 38, 40, and 50, and references therein). Therefore, only the  $(1)^3B_1 - \tilde{X}^1A_1$  and  $(1)^1B_1 - \tilde{X}^1A_1$  transitions of  $\text{SnCl}_2$  have been considered in the present study.

Secondly, only the symmetric stretching and bending vibrational modes have been considered in the present study, as the asymmetric stretching mode of  $b_2$  symmetry is only allowed with double quanta in an electronic transition between two states of  $C_{2v}$  symmetry. Also, it should be noted that, from published LIF and dispersed fluorescence spectra of  $\text{GeCl}_2$ ,<sup>31,83</sup> particularly based on the very recent study of Ref. 31, the only spectral feature, which has been tentatively as-

TABLE III. Computed relative electronic ( $T_v$ , vertical excitation) energies in eV (kcal mole<sup>-1</sup>) of low-lying singlet and triplet states of SnCl<sub>2</sub> obtained at different levels of calculation (the CAS/ $A_f$  and CASSCF/MRCI/A calculations were carried out at the RCCSD(T)/A optimized geometry of the  $\tilde{X}^1A_1$  state of SnCl<sub>2</sub>, while the CASSCF/MRCI/B and RCCSD(T)/B calculations were carried out at the RCCSD(T)/B optimized geometry of the  $\tilde{X}^1A_1$  state of SnCl<sub>2</sub>) (see Table I for the basis sets used).

State <sup>a</sup>	CAS <sup>b</sup> / $A_f$	CAS <sup>c</sup> /A	MRCI <sup>c,d</sup> /A	MRCI <sup>c,d</sup> /B	CCSD(T)/A	CCSD(T)/B
$^1A_1$	0	0	0	0	0	0
$^3B_1$	2.67	2.63	2.85	2.86	2.866	2.877
( $12a_1$ ) <sup>1</sup> ( $5b_1$ ) <sup>1</sup>			(65.7)	(66.0)	(66.1)	(66.3)
$^1B_1$	3.91	3.95	4.08	4.11		
( $12a_1$ ) <sup>1</sup> ( $5b_1$ ) <sup>1</sup>	[1.894] <sup>e</sup>		(94.2)	94.7		
$^3A_2$	4.56	4.77	4.81	4.84	4.801	4.831
( $5b_1$ ) <sup>1</sup> ( $9b_2$ ) <sup>1</sup>			(110.8)	(111.5)	(111.7)	(111.4)
$^1A_2$	4.58	4.78	4.78	4.81		
( $5b_1$ ) <sup>1</sup> ( $9b_2$ ) <sup>1</sup>			(110.2)	(110.9)		
$^3B_2$	4.78	5.34 <sup>f</sup>	4.92 <sup>f</sup>	<sup>g</sup>	4.988	5.020
( $5b_1$ ) <sup>1</sup> ( $3a_2$ ) <sup>1</sup>			(113.4)		(115.0)	(115.8)
$^1B_2$	5.08	5.33	5.17	5.22		
( $5b_1$ ) <sup>1</sup> ( $3a_2$ ) <sup>1</sup>	[1.689] <sup>e</sup>		(119.2)	(120.3)		
$^3A_1$	5.18	5.36	5.83	5.83	5.359	5.391
( $4b_1$ ) <sup>1</sup> ( $5b_1$ ) <sup>1</sup>			(134.4)	(134.3)	(123.6)	(124.3)
$^1A_1$		5.81 <sup>h</sup>	5.71 <sup>h</sup>			
( $4b_1$ ) <sup>1</sup> ( $5b_1$ ) <sup>1</sup>		[1.297] <sup>e</sup>	(131.6)			

<sup>a</sup>With the ECP28MDF ECP accounting for the  $1s2s2p3s3p3d$  shells of Sn, the  $\tilde{X}^1A_1$  state of SnCl<sub>2</sub> has the electronic configuration of  $\cdots(12a_1)^2(4b_1)^2(9b_2)^2(3a_2)^2$ . For each excited state, the main open-shell configuration with the largest computed CI coefficient,  $C_0^{\text{MRCI}}$ , in the MRCI wave function for that state is shown. The computed  $C_0^{\text{MRCI}}$  and the  $\Sigma(C_{\text{ref}})^2$  values obtained from the MRCI calculations for all states are larger than 0.88 and 0.93, respectively.

<sup>b</sup>Average-state CASSCF calculations with eight states: four lowest singlet states and four lowest triplet states of each symmetry of the  $C_{2v}$  point group.

<sup>c</sup>Single-state CASSCF/MRCI calculations for each state, except for the ( $2$ )<sup>1</sup> $A_1$  state (see footnote h).

<sup>d</sup>MRCI energies plus Davidson corrections.

<sup>e</sup>Computed transition dipole moments (in Debye) from average-state CASSCF calculations between excited singlet states and the  $\tilde{X}^1A_1$  state of SnCl<sub>2</sub> are in square brackets.

<sup>f</sup>The CASSCF calculation on the ( $1$ )<sup>3</sup> $B_2$  state with a full valence active space has convergence problems. These values are obtained employing an active space of the full valence plus one more  $a_2$  empty orbital for both the  $\tilde{X}^1A_1$  and ( $1$ )<sup>3</sup> $B_2$  states of SnCl<sub>2</sub>.

<sup>g</sup>CASSCF convergence problems with a full valence active space; see also footnote f and text.

<sup>h</sup>The results for the ( $2$ )<sup>1</sup> $A_1$  state are from two-state average-state CASSCF/MRCI calculations. i.e., the ( $1$ )<sup>1</sup> $A_1$  and ( $2$ )<sup>1</sup> $A_1$  states (see text).

signed to the asymmetric stretching mode of the  $\tilde{X}^1A_1$  state of Ge<sup>35</sup>Cl<sup>37</sup>Cl, is a weak peak observed in the dispersed fluorescence spectra; Ge<sup>35</sup>Cl<sup>37</sup>Cl is actually of  $C_s$  symmetry.<sup>31</sup> Since *ab initio* energy scans and FC factor calculations with the additional coordinate of the asymmetric stretching mode will require considerably more computational effort, it is felt that such a study would await the availability of an experimental spectrum, which shows the need to include the asymmetric stretching mode.

## RESULTS AND DISCUSSION

### Low-lying excited states of SnCl<sub>2</sub>

The computed vertical ( $T_v$ ) and adiabatic ( $T_e$ ) excitation energies of some low-lying excited states of SnCl<sub>2</sub> from the  $\tilde{X}^1A_1$  state, obtained at different levels of calculation, are summarized in Tables III and IV, respectively. Some details of these calculations are given in the footnotes of these tables. Before these results are discussed, the following points should be noted. Firstly, the main aim of this part of the present study is to obtain a general picture of the energy ordering (both adiabatically and vertically) of the low-lying excited states of SnCl<sub>2</sub>. Secondly, for the ( $2$ )<sup>1</sup> $A_1$  state, the  $T_v$  value was obtained from two-state average-state CASSCF/

MRCI calculations [i.e., the ( $1$ )<sup>1</sup> $A_1$  (or  $\tilde{X}^1A_1$ ) and ( $2$ )<sup>1</sup> $A_1$  states; see footnote h of Table III]. For the geometry optimization of the ( $2$ )<sup>1</sup> $A_1$  state, however, two-state average-state CASSCF calculations were followed by single-state MRCI calculations requesting only the second root. This is because the geometry of the ( $2$ )<sup>1</sup> $A_1$  state was optimized (see footnote c of Table IV) and two-state MRCI calculations involve a significantly larger configurational space than single-state MRCI calculations. Thirdly, for the evaluation of  $T_v$  of the ( $1$ )<sup>3</sup> $B_2$  state with the CASSCF/MRCI method, CASSCF calculations faced convergence problems with a full valence active space. In order to achieve convergence in the CASSCF calculations, one more virtual molecular orbital of  $a_2$  symmetry was added to the active space (see footnote g of Table III). The agreement between the computed  $T_v$  values of the ( $1$ )<sup>3</sup> $B_2$  state thus obtained (i.e., the MRCI+D values, see Table III) and those obtained at the RCCSD(T)/A level [i.e., the RCCSD(T) values; see Table III] is excellent, confirming the reliability of the CASSCF/MRCI results with the extra  $a_2$  molecular orbital in the active space. Lastly, computed  $T_1$  diagnostics and CI wave functions obtained from RCCSD(T) and MRCI calculations, respectively ( $T_1$  diagnostics and CI coefficients,  $C_0$ 's, are given in Table IV, see also footnote b of Table III), suggest insignificantly small CI

TABLE IV. The optimized geometrical parameters ( $r_e$  in Å and  $\theta_e$  in °), computed relative electronic energies ( $T_e$  in eV; relative to the  $\tilde{X}^1A_1$  state) of some low-lying excited singlet and triplet states of SnCl<sub>2</sub> obtained at different levels of calculation, computed  $T_1$  diagnostics [from RCCSD(T) calculations], and CI coefficients of the main configuration ( $C_0$ 's from MRCI calculations).

Methods; states and configuration	$r_e$	$\theta_e$	$T_e$		
RCCSD(T)/A			RCCSD	RCCSD(T)	$T_1$
$^3B_1(12a_1)^1(5b_1)^1(9b_2)^2(3a_2)^2$	2.3589	116.60	2.705	2.727	0.0172
$^3A_2(12a_1)^2(5b_1)^1(9b_2)^1(3a_2)^2$	2.6074	59.68	3.353	3.416	0.0109
$^3B_2(12a_1)^2(5b_1)^1(9b_2)^2(3a_2)^1$	2.6124	77.75	4.418	4.409	0.0123
$^3A_1(12a_1)^2(4b_1)^1(5b_1)^1(9b_2)^2(3a_2)^2$	2.6560	90.43	4.799	4.748	0.0136
RCCSD(T)/B					
$^3B_1(12a_1)^1(5b_1)^1(9b_2)^2(3a_2)^2$	2.3560	116.54	2.715	2.737	0.0170
$^3A_2(12a_1)^2(5b_1)^1(9b_2)^1(3a_2)^2$	2.6033	59.60	3.485	3.438	0.0108
RCCSD(T)/A1					
$^3B_1(12a_1)^1(5b_1)^1(9b_2)^2(3a_2)^2$	2.3272	117.30	2.803	2.850	0.0197
$^3A_2(12a_1)^2(5b_1)^1(9b_2)^1(3a_2)^2$	2.5657	60.66	3.460	3.422	0.0127
CASSCF/MRCI+D/A <sup>a</sup>			MRCI	MRCI+D	$C_0$ <sup>b</sup>
$^1A_2(12a_1)^2(5b_1)^1(9b_2)^1(3a_2)^2$	2.4644	66.66	3.843	3.820	0.9112
$^1B_1(12a_1)^1(5b_1)^1(9b_2)^2(3a_2)^2$	2.4065	115.12	3.966	3.978	0.9208
$^1B_2(12a_1)^2(5b_1)^1(9b_2)^2(3a_2)^1$	2.5431	84.73	4.789	4.720	0.8836
$^1A_1(12a_1)^2(4b_1)^1(5b_1)^1(9b_2)^2(3a_2)^{2c}$	2.5481	89.773	5.601	5.577	0.8460
CASSCF/MRCI+D/B <sup>a</sup>					
$^1A_2(12a_1)^2(5b_1)^1(9b_2)^1(3a_2)^2$	2.4617	66.20	3.856	3.834	0.9121
$^1B_1(12a_1)^1(5b_1)^1(9b_2)^2(3a_2)^2$	2.4017	115.18	3.983	3.998	0.9037
CASSCF/MRCI+D/A1 <sup>a</sup>					
$^1A_2(12a_1)^2(5b_1)^1(9b_2)^1(3a_2)^2$	2.5790	60.66	3.569	3.494	0.9058
$^1B_1(12a_1)^1(5b_1)^1(9b_2)^2(3a_2)^2$	2.3800	119.72	3.828	3.792	0.8989

<sup>a</sup>The CASSCF/MRCI and CASSCF/MRCI+D energies of the  $\tilde{X}^1A_1$  states computed at the RCCSD(T) optimized geometry of the  $\tilde{X}^1A_1$  state employing the same basis set were used to evaluate the  $T_e$  values of the excited states.

<sup>b</sup>The computed CI coefficient of the main configuration obtained from the MRCI calculation.

<sup>c</sup>This is the  $(2)^1A_1$  state; the  $(1)^1A_1$  state is the  $\tilde{X}^1A_1$  state. For the geometry optimization of the  $(2)^1A_1$  state, two-state (of  $A_1$  symmetry), average-state CASSCF calculations were carried out, followed by single-state MRCI calculations requesting for the second root; see text.

mixing in all electronic states considered. In this connection, a single-reference method, such as the RCCSD(T) method, should be adequate for the ground and low-lying excited triplet states.

Since vertical excitation energies ( $T_v$ ) are more relevant than adiabatic excitation energies ( $T_e$  or  $T_0$ ) for the identification of the molecular carrier of, and/or electronic states involved in, an absorption or LIF spectrum, the energy ordering in the vertical excitation region is first considered based on computed  $T_v$  values given in Table III. The lowest-lying excited triplet and singlet states of SnCl<sub>2</sub> are the  $(1)^3B_1$  and  $(1)^1B_1$  states, respectively. Above these two states are the  $(1)^3A_2$  and  $(1)^1A_2$  states, which are close to each other in energy (separated only by 0.03 eV) and are  $\sim 0.7$  eV higher in energy than the  $(1)^1B_1$  state. It should be noted that the computed  $T_v$  values of the triplet states considered, as shown in Table III, obtained by both the CASSCF/MRCI and RCCSD(T) methods and the two basis sets used are reasonably consistent, suggesting that the computed  $T_v$  values, and hence the energy ordering, should be reasonably reliable. However, based on the computed  $T_e$  values shown in Table IV, the ascending adiabatic energy ordering of the low-lying electronic states of SnCl<sub>2</sub> is  $\tilde{X}^1A_1$ ,  $\tilde{a}^3B_1$ ,  $\tilde{b}^3A_2$ ,  $\tilde{A}^1A_2$ ,  $\tilde{B}^1B_1$ ,  $\tilde{c}^3B_2$ ,  $\tilde{C}^1B_1$ ,  $\tilde{d}^3A_1$ , and  $\tilde{D}^1A_1$ . Adiabatically, the  $(1)^3A_2$  and

$(1)^1A_2$  states are in between the  $(1)^3B_1$  and  $(1)^1B_1$  states. From Table IV, it is clear that the  $\tilde{a}$  state is the  $(1)^3B_1$  state, because the  $T_e$  value of the  $(1)^3A_2$  state is computed to be consistently larger than that of the  $(1)^3B_1$  state by  $\sim 0.6$  eV at all levels of calculation. However, the differences between the computed  $T_e$  values of the  $(1)^1A_2$  and  $(1)^1B_1$  states are small, ranging between 0.15 and 0.30 eV at different levels of calculation. Nevertheless, from the results of our calculations as shown in Table IV, the  $(1)^1A_2$  state is computed to be consistently lower than the  $(1)^1B_1$  state adiabatically at all levels of calculation. Therefore, it is concluded that the low-lying singlet states of SnCl<sub>2</sub> have the order of  $\tilde{A}^1A_2$  and  $\tilde{B}^1B_1$ . This is similar to results obtained from our previous *ab initio* study on GeCl<sub>2</sub> where the  $T_e$  of the  $(1)^1A_2$  state was computed to be very close in energy to that of the  $(1)^1B_1$  state, and the suggestion that the  $\tilde{A}$  state of GeCl<sub>2</sub> may be the  $(1)^1A_2$  state.<sup>38</sup>

Regarding electronic excitations from the  $\tilde{X}^1A_1$  state of SnCl<sub>2</sub> to low-lying excited singlet states, the computed transition dipole moments between the  $(1)^1B_1$ ,  $(1)^1B_2$ , and  $(1)^1A_1$  states, and the  $\tilde{X}^1A_1$  state, obtained from average-state CASSCF calculations are given in Table III (in square brackets; see footnote f). They suggest that absorptions from

the  $\tilde{X}^1A_1$  state to all three excited singlet states should have appreciable intensities. The electronic excitation from the  $\tilde{X}^1A_1$  state to the  $(1)^1A_2$  state of SnCl<sub>2</sub>, which is dipole forbidden, has been discussed above, and this discussion will not be repeated here. In the following, we focus on the  $\tilde{X}^1A_1$ ,  $\tilde{a}^3B_1$ , and  $\tilde{B}^1B_1$  states of SnCl<sub>2</sub>, which are investigated by state-of-the-art *ab initio* calculations and considered for spectral simulation.

## GEOMETRICAL PARAMETERS AND VIBRATIONAL FREQUENCIES OF THE $\tilde{X}^1A_1$ STATE OF SnCl<sub>2</sub>

Optimized geometrical parameters and computed vibrational frequencies of the  $\tilde{X}^1A_1$  state of SnCl<sub>2</sub> are summarized and compared with available theoretical and experimental values in Table V. It is clear that calculations performed in the present study are of higher levels than previously reported, and also, a more systematic investigation has been carried out here. Therefore, we focus only on the results of our calculations. Firstly, when the computed bond angles ( $\theta_e$ ) obtained using the RCCSD(T) method with different basis sets are considered, including outer core electrons in the correlation treatment generally increases their values. However, basis set extension effects, as estimated from differences between results obtained employing basis sets of QZ (basis sets A, A1, A2, and A3; see Table I) and 5Z (basis sets B, B1, and B2) quality, decrease the computed bond angles. Also, the overall core correlation effects (i.e., the overall difference between with and without core correlation) with the larger 5Z quality basis sets are smaller than those with the QZ quality basis sets, but different core electrons with the 5Z basis sets have different and larger correlation effects on  $\theta_e$  from/than with the QZ basis sets. The relationship between core correlation and basis set size effects on the computed equilibrium bond angle of the  $\tilde{X}^1A_1$  state of SnCl<sub>2</sub> is complex and these effects do not appear to be simply additive. Nevertheless, the largest core correlation contributions appear to have come from the Sn  $4d^{10}$  electrons for both the QZ and 5Z basis sets used. In this connection, core correlation from Sn  $4s^24p^6$  and Cl  $2s^22p^6$  electrons may be ignored. In any case, the spread of the computed bond angles of the  $\tilde{X}^1A_1$  state of SnCl<sub>2</sub> obtained at different levels of calculation in the present study is very small (only  $0.4^\circ$ ), indicating highly consistent results. Based on the value obtained using basis set B2, the best estimate of the equilibrium bond angle of the  $\tilde{X}^1A_1$  state of SnCl<sub>2</sub> including corrections of core correlation and extrapolating to the CBS limit (see footnote b of Table V) is  $(97.52 \pm 0.16)^\circ$ . It is pleasing that the best theoretical estimate from the present study agrees very well with the experimentally derived value of  $(97.7 \pm 0.8)^\circ$  of Ref. 55 [from electron diffraction in conjunction with spectroscopic data for anharmonic diffraction analyses (ED+SP); see Table V and original work]. Other available experimental values seem to be too large, but they also have relatively larger uncertainties (see Table V).

Considering the computed equilibrium bond lengths ( $r_e$ ), both effects of core correlation and basis set extension lead to smaller values. However, basis set extension effects are

significantly smaller than core correlation effects. Similar to the discussion above on the computed  $\theta_e$  values, including correlation of the Sn  $4d^{10}$  core electrons has the largest core correlation effects on  $r_e$ , reducing its value by over  $0.03 \text{ \AA}$  with both QZ and 5Z quality basis sets. Based on the computed value employing basis set B2, the best theoretical estimate for  $r_e$  is  $2.3412 \pm 0.0052 \text{ \AA}$  (see footnote b of Table V). It is pleasing that this value agrees with all the available experimentally derived values to within the estimated theoretical uncertainty.

Harmonic vibrational frequencies of the  $\tilde{X}^1A_1$  state of SnCl<sub>2</sub> have been calculated employing three basis sets, namely, A, A1, and B. The largest spread of the computed values using different basis sets is  $4.2 \text{ cm}^{-1}$  for the bending mode (difference between using basis sets A and A1), which may be considered as the estimated theoretical uncertainties of the computed vibrational frequencies reported in this work. Fundamental vibrational frequencies have been computed variationally employing the RCCSD(T)/B PEF for the symmetric stretching and bending modes (Table V). Their values, when compared with the harmonic counterparts, suggest small anharmonicities associated with these two vibrational modes. The agreement between the computed fundamental frequencies with available experimental values is reasonably good, particular for the bending mode.

## GEOMETRICAL PARAMETERS AND VIBRATIONAL FREQUENCIES OF THE $\tilde{a}^3B_1$ AND $\tilde{B}^1B_1$ STATE-OF SnCl<sub>2</sub>

Considering first RCCSD(T) results of the  $\tilde{a}^3B_1$  state of SnCl<sub>2</sub> given in Table VI, the trends of both core correlation and basis set extension effects on computed  $\theta_e$  and  $r_e$  values are generally similar to those for the  $\tilde{X}^1A_1$  state discussed above. However, the spread of the computed  $\theta_e$  values of the  $\tilde{a}^3B_1$  state of  $0.75^\circ$  is nearly double that of the  $\tilde{X}^1A_1$  state, showing that the bond angle of the  $\tilde{a}^3B_1$  state is more sensitive to the level of calculation than that of the  $\tilde{X}^1A_1$  state. Nevertheless, based on the results obtained at the RCCSD(T)/B2 level, the best theoretical estimates for  $r_e$  and  $\theta_e$  of the  $\tilde{a}^3B_1$  state are  $2.3101 \pm 0.0076 \text{ \AA}$  and  $(117.29 \pm 0.06)^\circ$ , respectively (see footnote b of Table VI). No experimental values are available for comparison, and hence these best theoretical estimates are currently the most reliable geometrical parameters of the  $\tilde{a}^3B_1$  state of SnCl<sub>2</sub>.

Regarding the computed vibrational frequencies of the  $\tilde{a}^3B_1$  state of SnCl<sub>2</sub>, similar to those of the  $\tilde{X}^1A_1$  state discussed above, the difference between the computed harmonic and fundamental values are small, suggesting small anharmonicities for both the symmetric stretching and bending modes. Comparing theory with experiment, the calculated fundamental value of the bending mode obtained employing the RCCSD(T)/B PEF of  $85.4 \text{ cm}^{-1}$  agrees reasonably well with the only available experimental value of  $80 \pm 5 \text{ cm}^{-1}$ ,<sup>53</sup> supporting the assignment of the vibrational structure observed in the emission spectrum to the bending mode of the  $\tilde{a}^3B_1$  state of SnCl<sub>2</sub>. However, the computed fundamental frequency of the symmetric stretching mode of  $348.2 \text{ cm}^{-1}$

TABLE V. The optimized geometrical parameters ( $r_e$  in Å and  $\theta_e$  in °) and computed harmonic vibrational frequencies ( $\omega_e$ 's; fundamental frequencies in square brackets; in  $\text{cm}^{-1}$ ) of the  $\tilde{X}^1A_1$  state of  $\text{SnCl}_2$  obtained at the different levels of calculation, those from previous calculations (relatively higher levels only; see text), and available experimental values.

Basis/methods	$r_e$	$\theta_e$	$\omega_e (a_1, a_1, b_2)^a$
RCCSD(T)/A	2.3860	97.65	361.4, 118.6, 345.5
RCCSD(T)/A1	2.3548	97.90	362.6, 122.8, 345.5
RCCSD(T)/A2	2.3539	97.92	
RCCSD(T)/A3	2.3510	97.88	
RCCSD(T)/B	2.3834	97.60	363.0, 118.1, 347.1
RCCSD(T)/B PEF	2.3834	97.63	364.9, 119.9, – [363.6, 119.8, –]
RCCSD(T)/B1	2.3503	97.75	
RCCSD(T)/B2	2.3464	97.68	
Best estimate (CBS+core) <sup>b</sup>	2.3412	97.52	
SCF/MRCI/[2s2p1d] <sup>c</sup>	2.362	99.7	[368, 124, 371]
CAS/MRCI/ECP-[3s3p1d],-[4s4p1d] <sup>d</sup>	2.363	98.4	
B3LYP/ECP <sup>e</sup>	2.417	98.9	
LSD <sup>f</sup>	2.395	99.4	356, 118, 376
NLSD-PP <sup>f</sup>	2.422	103	305, 33, 331
CCSD(T)/EC <sup>g,h</sup>	2.357	98.4	
CCSD(T)/ST <sup>h,i</sup>	2.380	98.4	
CCSD(T)/ECP2; <sup>j</sup> aug-cc-pVTZ <sup>k</sup>	2.384	98.1	
MP2/ECP2; <sup>j</sup> aug-cc-pVQZ <sup>k</sup>	2.334	98.4	
MP2/ECP2; <sup>j</sup> aug-cc-pVTZ <sup>k</sup>	2.379	97.8	345, 122, 337
CCSD(T)/SDB_cc-pVTZ, cc-pVTZ <sup>l</sup>	2.3802	98.3	339, 123, 354
MP2/SDB_aug-cc-pVTZ <sup>m,n</sup>	2.375	97.6	359.1, 147.6, 337.1
B3LYP/SDB_aug-cc-pVTZ <sup>m,n</sup>	2.398	98.8	
MP2/SDD; 6-311+G <sup>o</sup>	2.417	98.2	
ED ( $r_e$ compilation) <sup>p</sup>	2.347(7)	99(1)	
ED (thermal average: $r_e$ ) <sup>q</sup>	2.345(3)	98.5(20)	
ED (estimated $r_e$ ) <sup>f</sup>	2.335(3)	98.1	
ED+SP <sup>s</sup> ( $r_e$ ) <sup>r</sup>	2.338(3)	97.7(8)	
ED+SP <sup>s</sup> ( $r_e$ ) <sup>t</sup>	2.335(3)	99.1(20)	
Emission <sup>u</sup>			[355, 122]
Emission <sup>v</sup>			[350, 120]
Raman <sup>w</sup>			[351, 120, 330]
Raman (514.5 nm; at 690 and 1024 K) <sup>x</sup>			[362, 127, 344]
Raman (488 nm; at 690–1024 K) <sup>x</sup>			[355, 121, 347]
Raman (457.9 nm; at 666, 690, and 1042 K) <sup>x</sup>			[358, 121, 340]

<sup>a</sup>Symmetric stretching, bending, and asymmetric stretching modes.

<sup>b</sup>Based on the RCCSD(T)/B2 values, the correction to the complete basis set (CBS) limit was estimated by half of the difference between the values obtained using basis sets B2 and A2. The correction of the core correlation of Cl  $2s^2 2p^6$  electrons was estimated by the difference between the values obtained using the A3 and A2 basis sets. These corrections are assumed to be additive. The estimated theoretical uncertainties are  $\pm 0.0052$  Å and  $\pm 0.16^\circ$ , based on the difference between the best estimates and those obtained using the B2 basis set.

<sup>c</sup>Reference 64.

<sup>d</sup>Reference 65.

<sup>e</sup>Reference 70.

<sup>f</sup>Reference 66.

<sup>g</sup>A relativistic ECP with the [4s4p1d], and cc-pVTZ basis set for Sn and Cl, respectively.

<sup>h</sup>Reference 67.

<sup>i</sup>The ECP46MWB with the [3s3p2d1f], and cc-pVTZ basis set for Sn and Cl, respectively.

<sup>j</sup>The ECP2 basis set consists of the ECP46MWB ECP and the aug-cc-pVQZ basis set for Sn.

<sup>k</sup>Reference 69.

<sup>l</sup>Reference 68.

<sup>m</sup>The aug-cc-pVTZ basis set was used for Cl. However,  $f$  functions were excluded and six-component  $d$  functions were used.

<sup>n</sup>Reference 71.

<sup>o</sup>Reference 72.

<sup>p</sup>Reference 85.

<sup>q</sup>Reference 56.

<sup>r</sup>Reference 55.

<sup>s</sup>From electron diffraction in conjunction with spectroscopic data for anharmonic diffraction analyses.

<sup>t</sup>Reference 57.

<sup>u</sup>Reference 52.

<sup>v</sup>Reference 53.

<sup>w</sup>Reference 54.

<sup>x</sup>Reference 58.



TABLE VI. The optimized geometrical parameters ( $r_e$  in Å and  $\theta_e$  in °), computed harmonic vibrational frequencies ( $\omega_e$ 's in cm<sup>-1</sup> and fundamental frequencies in square brackets), and relative electronic energies,  $T_e$ , in eV (cm<sup>-1</sup>) of the  $\tilde{a}^3B_1$  and  $\tilde{A}^1B_2$  states of SnCl<sub>2</sub> obtained at different levels of calculation and from previous computational (relatively higher levels only; see text) and experimental studies.

$\tilde{a}^3B_1$	$r_e$	$\theta_e$	$\omega_e (a_1, a_1, b_2)^a$	$T_e$
CAS/MRCI+D/A	2.3399	114.52		2.709 (21 851)
CAS/MRCI+D/A1	2.3495	117.22		2.951 (23 8.03)
CAS/MRCI+D/B	2.3368	114.50		2.721 (21 950)
RCCSD(T)/A	2.3589	116.60	346.5, 84.9, 375.5	2.727 (21 994)
RCCSD(T)/A1	2.3272	117.30		2.850 (22 989)
RCCSD(T)/A2	2.3263	117.35		2.875 (23 185)
RCCSD(T)/A3	2.3231	117.30		2.878 (23 212)
RCCSD(T)/B	2.3560	116.54	348.4, 85.2, 377.5	2.737 (22 078)
RCCSD(T)/B PEF	2.3560	116.85	350.1, 84.3, - [348.2, 85.4, -]	
RCCSD(T)/B1	2.3218	117.21		2.860 (23 066)
RCCSD(T)/B2	2.3176	117.34		2.881 (23 239)
Best estimate (CBS+core) <sup>b</sup>	2.3101	117.29		2.888 (23 293)
Best $T_0^c$				2.887 (23 284)
CASSCF/ECP-[3s3p1d],-[4s4p1d] <sup>d</sup>	2.362	115.0		2.48
CAS/MRCI/ECP-[3s3p1d],[4s4p1d] <sup>d</sup>	2.336	116.0		2.60
LSD <sup>e</sup>	2.381	117.4		2.68
NLSD-PP <sup>e</sup>	2.424	124.4	336, 136, 361	2.47
UCCSD(T)/EC <sup>f,g</sup>	2.326	116.6		2.61
UCCSD(T)/ST <sup>g,h</sup>	2.357	117.3		2.68
Emission <sup>i</sup>				2.757 (22 237)
Emission <sup>j</sup>			[240(5), 80(5), -]	2.759 (22 249)
$\tilde{A}^1B_1$				
CAS/MRCI+D/A	2.4065	115.12		3.978 (32 088)
CAS/MRCI+D/A PEF	2.4061	115.21	280.4, 79.7, - [278.7, 79.4, -]	
CAS/MRCI+D/A1	2.3800	119.72		3.792 (30 582)
CAS/MRCI+D/B	2.4016	115.18		3.978 (32 243)
Best estimate (CBS+core) <sup>k</sup>	2.3727	119.81		3.821 (30 815)
Best $T_0^l$				3.813 (30 752)
CASSCF/ECP-[3s3p1d],-[4s4p1d] <sup>d</sup>	2.484	119.7		
CAS-MRCI/ECP-[3s3p1d],-[4s4p1d] <sup>d</sup>	2.418	118.8		

<sup>a</sup>Symmetric stretching, bending and asymmetric stretching modes.

<sup>b</sup>Based on the RCCSD(T)/B2 values, the correction to the complete basis set (CBS) limit was estimated by half of the difference between the values obtained using basis sets B2 and A2. The correction of the core correlation of C1 2s<sup>2</sup>2p<sup>6</sup> electrons was estimated by the difference between the values obtained using the A3 and A2 basis sets. These corrections are assumed to be additive. The estimated theoretical uncertainties for the best  $r_e$ ,  $\theta_e$ , and  $T_e$  values are  $\pm 0.0076$  Å,  $\pm 0.06^\circ$ , and  $\pm 0.007$  eV (54 cm<sup>-1</sup>), respectively, based on the differences between the best estimated values and those obtained using basis set B2.

<sup>c</sup>The computed harmonic frequencies of all three vibrational modes obtained at the RCCSD(T)/B level of calculation (Tables III and IV) were used for the zero-point vibrational energy correction.

<sup>d</sup>Reference 65.

<sup>e</sup>Reference 66.

<sup>f</sup>See footnote c of Table IV.

<sup>g</sup>Reference 67.

<sup>h</sup>See footnote d of Table IV.

<sup>i</sup>Reference 52.

<sup>j</sup>Reference 53.

<sup>k</sup>Based on the CASSCF/MRCI+D/B values, the correction to the complete basis set (CBS) limit was estimated by half of the difference between the values obtained using basis sets B and A. The correction of the core correlation of Sn 4d<sup>10</sup> electrons was estimated by the difference between the values obtained using the A1 and A basis sets. These corrections are assumed to be additive. The estimated theoretical uncertainties for the best  $r_e$ ,  $\theta_e$ , and  $T_e$  values are  $\pm 0.029$  Å,  $4.63^\circ \pm 0.06^\circ$ , and  $\pm 0.18$  eV (1430 cm<sup>-1</sup>), respectively, based on the difference between the best estimated values and those obtained using basis set B; see text.

<sup>l</sup>The computed fundamental frequencies of the two symmetric vibrational modes obtained from the RCCSD(T)/B and RASSCF/MRCI+D/A PEFs of the  $\tilde{X}^1A_1$  and  $\tilde{B}^1B_1$  states of SnCl<sub>2</sub> (Tables II and III) were used for the zero-point vibrational energy correction.

disagrees with the only available experimental value of 240 cm<sup>-1</sup> obtained from the same emission spectrum.<sup>53</sup> It has been noted above in the Introduction that a DFT study<sup>66</sup> has reported computed harmonic vibrational frequencies of the  $\tilde{a}^3B_1$  state of SnCl<sub>2</sub>. In this study, two functionals, namely, local density approximation (LSD) and NLSD-PP [a non-

local functional consisting of the exchange functional of Perdew and the correlation functional of Perdew and Yang (see Ref. 66)], were employed (see Table VI). If our speculation of some typing errors in the published article,<sup>66</sup> as mentioned above, is correct, the LDA functional would give  $\omega_1$ ,  $\omega_2$ , and  $\omega_3$  values of 336, 136, and 361 cm<sup>-1</sup>, while the

NLSD-PP functional gives values of 370, 58, and 382  $\text{cm}^{-1}$ , respectively, for the  $\tilde{a}^3B_1$  state of  $\text{SnCl}_2$ . Based on these DFT values, it appears that the computed  $\omega_2$  values are very sensitive to the functionals used and hence their reliability is doubtful. Nevertheless, all the computed  $\omega_1$  and/or  $\nu_1$  values of the  $\tilde{a}^3B_1$  state of  $\text{SnCl}_2$ , whether from the present *ab initio* or previous DFT study, are considerably larger than the experimental value of 240  $\text{cm}^{-1}$  obtained from the emission spectrum of Ref. 53. Further spectroscopic investigation is clearly required in order to establish the symmetric stretching vibrational frequency of the  $\tilde{a}^3B_1$  state of  $\text{SnCl}_2$  (see also the last section).

Before computed results of the  $\tilde{B}^1B_1$  state of  $\text{SnCl}_2$  are considered, it should be noted that geometry optimization calculations have also been carried out on the  $\tilde{a}^3B_1$  state employing the CASSCF/MRCI method using basis sets A, A1, and B. These results for the  $\tilde{a}^3B_1$  state, given also in Table VI, are for the purpose of accessing the reliability of the CASSCF/MRCI method for calculations on the  $\tilde{B}^1B_1$  state. This is firstly because the CASSCF/MRCI method is computationally significantly more demanding than the RCCSD(T) method (with the same basis set). Consequently, CASSCF/MRCI calculations on the open-shell singlet  $\tilde{B}^1B_1$  state with basis sets larger than basis sets A1 and/or B are beyond the computational capacity available to us. Secondly, the MRCI method is not size consistent, but the RCCSD(T) method is. Since it has been concluded above that triplet states considered in the present study can be studied adequately with a single-reference method, the RCCSD(T) method, which is size consistent, should be reliable and its results can serve as benchmarks to assess the reliability of the CASSCF/MRCI+D results of the  $\tilde{a}^3B_1$  state. In this connection, comparison between CASSCF/MRCI+D and RCCSD(T) results of the  $\tilde{a}^3B_1$  state would shed some light on the reliability of the CASSCF/MRCI+D results of the  $\tilde{B}^1B_1$  state, which cannot be studied using the single-reference RCCSD(T) method. The CASSCF/MRCI+D and RCCSD(T) results of the  $\tilde{a}^3B_1$  state of  $\text{SnCl}_2$  employing basis sets A, A1, and B are compared in Table VI. Summarizing, the best estimated  $r_e$  and  $\theta_e$  values of the  $\tilde{a}^3B_1$  state of  $\text{SnCl}_2$  based on the CASSCF/MRCI+D results shown in Table VI are  $2.3449 \pm 0.0081$  Å and  $(117.19 \pm 2.69)^\circ$ , respectively (i.e., including core correlation and basis set extension corrections following the same way as for the  $\tilde{B}^1B_1$  state to be discussed; see footnote e of Table VI). If the best estimated RCCSD(T) geometrical parameters of the  $\tilde{a}^3B_1$  state of 2.3101 Å and  $117.29^\circ$  obtained above are used as benchmarks for comparison, the differences of  $\pm 0.0348$  Å and  $\pm 0.10^\circ$ , between these best estimated RCCSD(T) and corresponding CASSCF/MRCI+D values, may be considered as more reliable theoretical uncertainties associated with the best estimated CASSCF/MRCI+D values of  $r_e$  and  $\theta_e$  for both the  $\tilde{a}^3B_1$  state and also the  $\tilde{B}^1B_1$  state to be discussed below.

Considering the CASSCF/MRCI+D results of the  $\tilde{B}^1B_1$  state of  $\text{SnCl}_2$  (see Table VI), while basis set extension effects (from basis sets of QZ to 5Z quality; i.e., basis sets A and B, respectively) on the computed  $r_e$  and  $\theta_e$  values are

insignificantly small, core correlation effects (differences between using basis sets A and A1) on them are considerable, particularly on the calculated equilibrium bond angle. Including Sn  $4d^{10}$  outer core electrons in the active space (with basis set A1) gives a computed  $\theta_e$  value of over  $4.5^\circ$  larger than that when the Sn  $4d^{10}$  electrons were frozen in the CASSCF/MRCI calculations (with basis set A). This increase in the computed  $\theta_e$  value for the  $\tilde{B}^1B_1$  state can be compared with a similar increase of  $2.7^\circ$  for the  $\tilde{a}^3B_1$  state with the CASSCF/MRCI method, but a significantly smaller increase of  $0.7^\circ$  with the RCCSD(T) method for the  $\tilde{a}^3B_1$  state. In summary, the best estimated  $r_e$  and  $\theta_e$  values of the  $\tilde{B}^1B_1$  state obtained based on the CASSCF/MRCI+D results are  $2.373 \pm 0.029$  Å and  $(119.81 \pm 4.63)^\circ$ , respectively (see footnote e of Table VI). However, if the more reliable uncertainties associated with the best estimated CASSCF/MRCI+D geometrical parameters obtained above for the  $\tilde{a}^3B_1$  state are transferable to the  $\tilde{B}^1B_1$  state, the theoretical uncertainty associated with the best estimated CASSCF/MRCI+D  $\theta_e$  value of the  $\tilde{B}^1B_1$  state should be significantly smaller than the rather large uncertainty of  $\pm 4.63^\circ$ , obtained based on CASSCF/MRCI+D results.

#### COMPUTED $T_e$ AND $T_0$ VALUES OF THE $\tilde{a}^3B_1$ AND $\tilde{B}^1B_1$ STATES OF $\text{SnCl}_2$

The computed  $T_e$  values of the  $\tilde{a}^3B_1$  and  $\tilde{B}^1B_1$  states of  $\text{SnCl}_2$  obtained at different levels of calculation are also summarized in Table VI. Considering RCCSD(T) results of the  $\tilde{a}^3B_1$  state first, basis set extension effects (differences between results employing QZ and 5Z quality basis sets) increase the computed  $T_e$  values, but only by  $\sim 0.01$  eV at the RCCSD(T) level. However, core correlation effects on computed  $T_e$  values are considerably larger, increasing their values by  $\sim 0.13$  eV. The major part of this increase arises from correlation of Sn  $4d^{10}$  electrons, similar to the conclusion made above on core correlation effects on computed geometrical parameters. The best theoretical estimate of the  $T_e$  value of the  $\tilde{a}^3B_1$  state of  $\text{SnCl}_2$  based on the present investigation is  $2.888 \pm 0.007$  eV ( $23\,293 \pm 54$   $\text{cm}^{-1}$ ; see footnote e of Table VII). Correcting for zero-point vibrational energies (ZPVEs) employing the computed RCCSD(T)/B harmonic vibrational frequencies of the two states (see Tables V and VI) gives the best  $T_0$  value of 2.887 eV ( $23\,284$   $\text{cm}^{-1}$ ). Comparing this value with available experimental  $T_0$  values of 2.757 eV ( $22\,237$   $\text{cm}^{-1}$ ) (Ref. 52) and 2.759 eV ( $22\,249$   $\text{cm}^{-1}$ ) (Ref. 53) obtained from emission spectra, it appears that the experimental values are too small by  $\sim 0.13$  eV ( $1050$   $\text{cm}^{-1}$ ). Since the bond angle of the  $\tilde{a}^3B_1$  state is computed to be larger than that of the  $\tilde{X}^1A_1$  state by  $\sim 20^\circ$  (see Tables V and VI), the  $\tilde{a}(0,0,0)$ - $\tilde{X}(0,0,0)$  region of the emission spectrum is therefore expected to be weak. In fact, computed FC factors of the  $\tilde{a}(0,0,0)$ - $\tilde{X}$  SVL emission obtained in the present study give the vibrational component  $\tilde{a}(0,0,0)$ - $\tilde{X}(0,11,0)$  at  $21\,968$   $\text{cm}^{-1}$  the maximum relative intensity (set to a computed FC factor of 1.0) and suggest that the  $\tilde{a}(0,0,0)$ - $\tilde{X}(0,0,0)$  vibrational component at

23 284 cm<sup>-1</sup> would be too weak to be observed (with a computed FC factor of 0.000 036). If the observed emission spectra of Refs. 52 and 53 were emitting from the (0,0,0) vibrational level of the  $\tilde{a}^3B_1$  state of SnCl<sub>2</sub> and the observed bands correspond to the regions of maximum intensity, then the vibrational quantum numbers associated with the observed vibrational structure should be significantly larger than those given in Refs. 52 and 53. Comparing the energy positions of emission lines obtained from the emission spectra reported in Refs. 52 and 53 with our *ab initio*/FC results, those assigned to the  $\tilde{a}(0,0,0)$ - $\tilde{X}(0,2,0)$  component in the emission spectra at 22 005 (Ref. 52) and 22 025 (Ref. 53) cm<sup>-1</sup> agree very well (within 0.007 eV or 57 cm<sup>-1</sup>) with the computed position of 21 968 cm<sup>-1</sup> for the  $\tilde{a}(0,0,0)$ - $\tilde{X}(0,11,0)$  component with the largest computed FC factor. Based on this comparison, we speculate that the vibrational assignments in  $\nu'_2$  of the emission spectra given in Refs. 52 and 53 are probably too small by nine quanta (i.e., if the molecular carrier is indeed SnCl<sub>2</sub>; *infra vide*). Further spectroscopic investigation is required to establish the vibrational assignments and the  $T_0$  position of the  $\tilde{a}$ - $\tilde{X}$  band system of SnCl<sub>2</sub> (see also the last section).

Regarding computed  $T_e$  values of the  $\tilde{B}^1B_1$  state of SnCl<sub>2</sub>, based on the CASSCF/MRCI+D/B value, the best  $T_e$  value is estimated to be 3.821±0.18 eV (30815 ±1430 cm<sup>-1</sup>; see footnote k of Table VI). Correcting for ZPVEs using the computed fundamental frequencies of the symmetric stretching and bending modes obtained from the PEFs of the two states, a best  $T_0$  value of 3.813 eV (30 752 cm<sup>-1</sup>) is obtained. However, no experimental value is available for comparison. Nevertheless, for the  $\tilde{a}^3B_1$  state, both computed RCCSD(T) and CASSCF/MRCI  $T_e$  values have been obtained (Table VI). The best CASSCF/MRCI  $T_e$  value estimated for the  $\tilde{a}^3B_1$  state (following the same way as for the  $\tilde{B}^1B_1$  state; see footnote k of Table VI) is 2.969±0.248 eV (23 952±2002 cm<sup>-1</sup>). Comparing this value with the corresponding best RCCSD(T) value of 2.888 eV (23 293 cm<sup>-1</sup>), the difference is 0.082 eV (659 cm<sup>-1</sup>). This difference between the best CASSCF/MRCI+D and RCCSD(T)  $T_e$  values for the  $\tilde{a}^3B_1$  state may be considered as a more realistic uncertainty associated with the best CASSCF/MRCI  $T_e$  value of the  $\tilde{B}^1B_1$  state.

### FRANCK-CONDON SIMULATION OF THE ABSORPTION AND SVL EMISSION SPECTRA OF SnCl<sub>2</sub>

The fitted polynomials of the PEFs used in the variational calculations of the anharmonic vibrational wave functions of the  $\tilde{X}^1A_1$ ,  $\tilde{a}^3B_1$ , and  $\tilde{B}^1B_1$  states of SnCl<sub>2</sub> are available from the authors. The root-mean-square deviations of these fitted PEFs from the *ab initio* data are 8.2, 10.4, and 3.1 cm<sup>-1</sup>, respectively. Some representative simulated spectra are given in Figs. 1–5. Each vibrational component of the absorption or SVL emission spectrum has been simulated with a Gaussian line shape and a full width at half maximum (FWHM) of 0.1 or 1.0 cm<sup>-1</sup>, respectively. In all spectral simulations, the best theoretical  $T_0$  values and best estimated

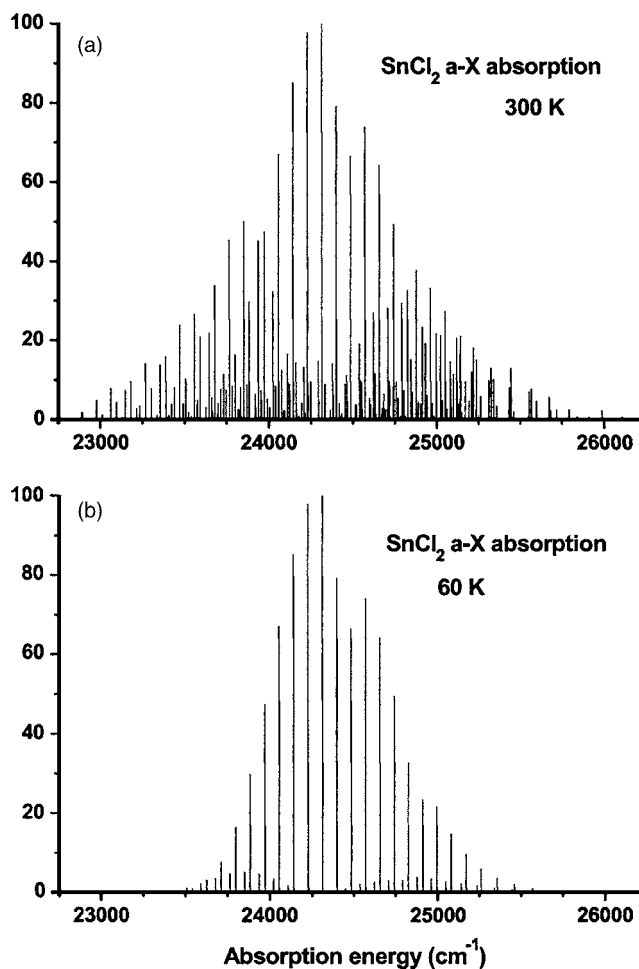


FIG. 1. Simulated  $\tilde{a}$ - $\tilde{X}$  absorption spectra of SnCl<sub>2</sub> with a  $T_0$  value of 23 284.4 cm<sup>-1</sup>, a FWHM of 0.1 cm<sup>-1</sup> for each vibrational component, and vibrational temperatures of (a) 60 (bottom trace) and (b) 300 K (top trace); see text for details.

geometrical parameters of each state were used, thus giving the best “theoretical” spectra.

In Fig. 1, the  $\tilde{a}^3B_1$ - $\tilde{X}^1A_1$  absorption spectra simulated with vibrational temperatures of 60 and 300 K (assuming a Boltzmann distribution for the populations of low-lying vibrational levels of the  $\tilde{X}^1A_1$  state) are shown. With a vibrational temperature of 60 K (Fig. 1, bottom trace), the major vibrational structure of the  $\tilde{a}$ - $\tilde{X}$  absorption band of SnCl<sub>2</sub> is due to the  $\tilde{a}(0, \nu'_2, 0)$ - $\tilde{X}(0,0,0)$  progression, which has the  $\nu'_2=12$  vibrational component at 24 314 cm<sup>-1</sup> having the largest computed FC factor (the vibrational component in a spectral band with the maximum computed FC factor has been set to 100% relative intensity in all the figures). As can be seen in Fig. 1 (bottom trace), the  $\tilde{a}(0,0,0)$ - $\tilde{X}(0,0,0)$  component at 23 284 cm<sup>-1</sup> is too weak to be observed. The first identifiable vibrational component of this progression is with  $\nu'_2=3$  at 23 540 cm<sup>-1</sup>, though the  $\tilde{a}(0,4,0)$ - $\tilde{X}(0,1,0)$  “hot band” vibrational component at 23 507 cm<sup>-1</sup>, which has a slightly larger computed FC factor than the  $\tilde{a}(0,3,0)$ - $\tilde{X}(0,0,0)$  component of the main progression, is most likely the first identifiable vibrational component of the whole absorption band at 60 K. The weak vibrational feature

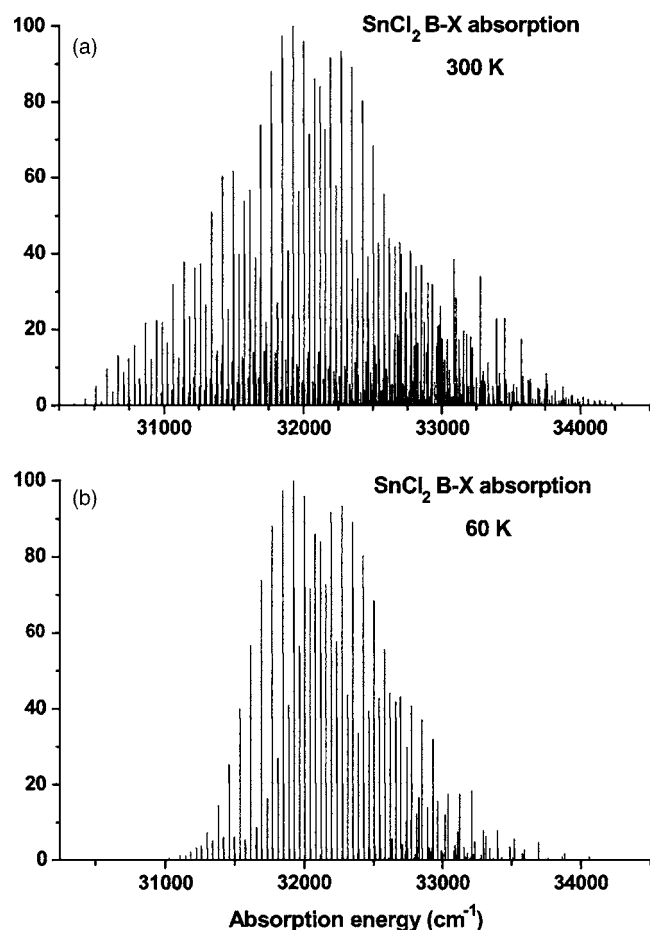


FIG. 2. Simulated  $\tilde{B}-\tilde{X}$  absorption spectra of  $\text{SnCl}_2$  with a  $T_0$  value of  $30\,752.3\text{ cm}^{-1}$ , a FWHM of  $0.1\text{ cm}^{-1}$  for each vibrational component, and vibrational temperatures of (a) 60 (bottom trace) and (b) 300 K (top trace); see text for details.

underneath the main  $\tilde{a}(0, \nu'_2, 0)-\tilde{X}(0, 0, 0)$  progression is the hot band progression,  $\tilde{a}(0, \nu'_2, 0)-\tilde{X}(0, 1, 0)$ . The  $\tilde{a}(1, \nu'_2, 0)-\tilde{X}(0, 0, 0)$  progression with  $\nu'_2 < 7$  is in general weaker than the  $\tilde{a}(0, \nu'_2, 0)-\tilde{X}(0, 1, 0)$  hot band series. However, for  $\nu'_2 \geq 7$ , the  $\tilde{a}(0, \nu'_2+4, 0)-\tilde{X}(0, 0, 0)$  and  $\tilde{a}(1, \nu'_2, 0)-\tilde{X}(0, 0, 0)$  vibrational components are very close in energy, and the  $\tilde{a}(0, \nu'_2+4, 0)$  and  $\tilde{a}(1, \nu'_2, 0)$  anharmonic vibrational wave functions are heavily mixed. In these cases, Fermi resonances have affected the relative intensities of both series, as shown in some irregularities in the main vibrational structure in Fig. 1 (bottom trace). With a vibrational temperature of 300 K (Fig. 1 top trace), in addition to the  $\tilde{a}(0, \nu'_2, 0)-\tilde{X}(0, 1, 0)$  hot band progression, more hot band progressions become observable, namely,  $\tilde{a}(0, \nu'_2, 0)-\tilde{X}(0, 2, 0)$ ,  $\tilde{a}(0, \nu'_2, 0)-\tilde{X}(0, 3, 0)$ ,  $\tilde{a}(0, \nu'_2, 0)-\tilde{X}(1, 0, 0)$ ,  $\tilde{a}(0, \nu'_2, 0)-\tilde{X}(0, 4, 0)$ , and  $\tilde{a}(0, \nu'_2, 0)-\tilde{X}(1, 1, 0)$  and the first identifiable vibrational component is  $\tilde{a}(0, 1, 0)-\tilde{X}(0, 4, 0)$  at  $22\,890\text{ cm}^{-1}$ .

The simulated  $\tilde{B}-\tilde{X}$  absorption spectra of  $\text{SnCl}_2$  with vibrational temperatures of 60 and 300 K are shown in Fig. 2 (bottom and top traces, respectively). It can be seen that the  $\tilde{B}-\tilde{X}$  band system is much more complex than the  $\tilde{a}-\tilde{X}$  band

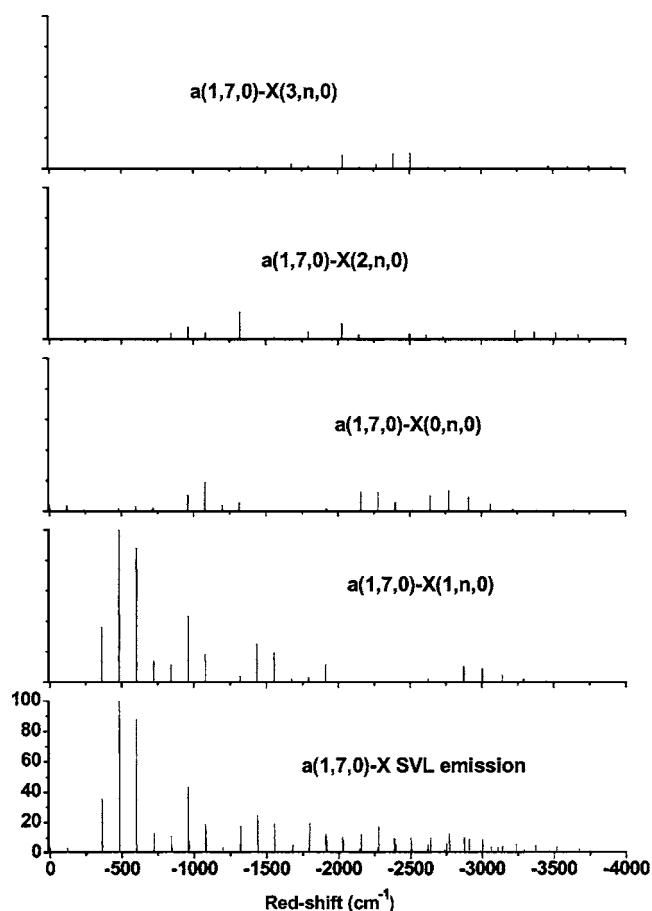


FIG. 3. The simulated  $\tilde{a}(1, 7, 0)-\tilde{X}$  SVL emission spectrum of  $\text{SnCl}_2$ , resulting from an excitation energy of  $24\,229.49\text{ cm}^{-1}$  from the  $\tilde{X}(0, 0, 0)$  level, with a FWHM of  $1\text{ cm}^{-1}$  for each vibrational component; the computed Franck-Condon factors of some major vibrational progressions are shown as bar diagrams above the simulated SVL emission spectrum (see text for details).

system. Nevertheless, the main vibrational structure consists mainly of three vibrational progressions, namely,  $\tilde{B}(0, \nu'_2, 0)-\tilde{X}(0, 0, 0)$ ,  $\tilde{B}(1, \nu'_2, 0)-\tilde{X}(0, 0, 0)$ , and  $\tilde{B}(2, \nu'_2, 0)-\tilde{X}(0, 0, 0)$ . The strongest vibrational components of these three series are  $\tilde{B}(0, 15, 0)-\tilde{X}(0, 0, 0)$ ,  $\tilde{B}(1, 16, 0)-\tilde{X}(0, 0, 0)$ , and  $\tilde{B}(2, 17, 0)-\tilde{X}(0, 0, 0)$  at  $31\,928$ ,  $32\,275$ , and  $32\,621\text{ cm}^{-1}$  with computed FC factors of 1.0, 0.933, and 0.44, respectively. The  $\tilde{B}(3, \nu'_2, 0)-\tilde{X}(0, 0, 0)$  and  $\tilde{B}(4, \nu'_2, 0)-\tilde{X}(0, 0, 0)$  progressions are predicted to be observable, but with significantly weaker relative intensities. The hot band series  $\tilde{B}(0, \nu'_2, 0)-\tilde{X}(0, 1, 0)$  is even weaker with a vibrational temperature of 60 K. However, the first identifiable vibrational component is the hot band component  $\tilde{B}(1, 1, 0)-\tilde{X}(0, 1, 0)$  at  $31\,028\text{ cm}^{-1}$ . Similar to the  $\tilde{a}-\tilde{X}$  band discussed above, the  $\tilde{B}(0, 0, 0)-\tilde{X}(0, 0, 0)$  vibrational component is too weak to be observed. Also, similar to above, with a vibrational temperature of 300 K, hot bands arising from excited vibrational levels, (0,1,0), (0,2,0), (0,3,0), (1,0,0), (0,4,0), and (1,1,0) of the  $\tilde{X}^1A_1$  state of  $\text{SnCl}_2$ , are predicted in the absorption spectrum.

The  $\tilde{a}(1, 7, 0)-\tilde{X}$  and  $\tilde{a}(0, 11, 0)-\tilde{X}$  SVL emission spectra,

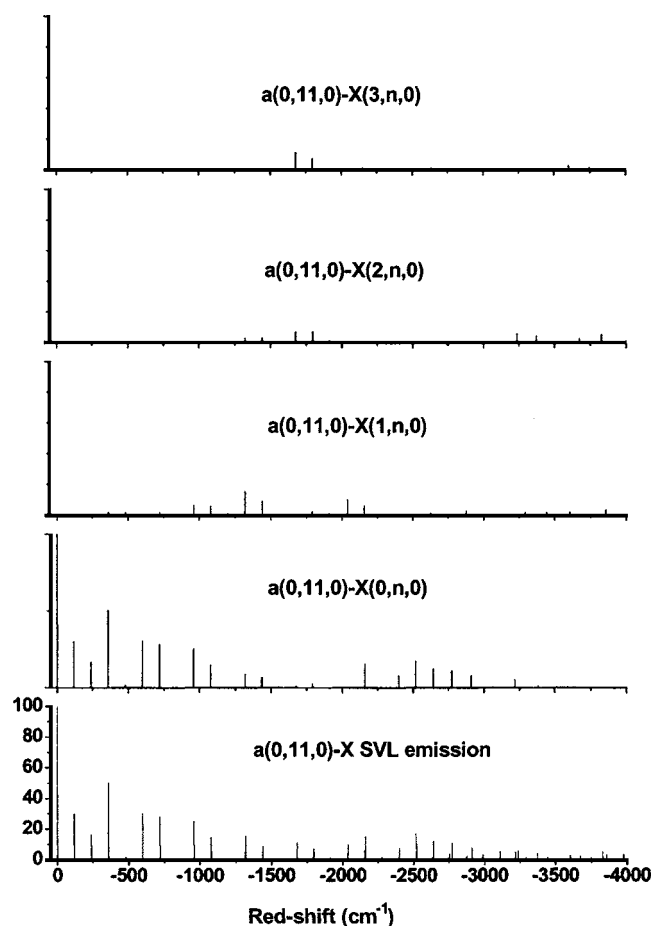


FIG. 4. The simulated  $\tilde{a}(0,11,0)-\tilde{X}$  SVL emission spectrum of SnCl<sub>2</sub> resulting from an excitation energy of 24 228.63 cm<sup>-1</sup> from the  $\tilde{X}(0,0,0)$  level with a FWHM of 1 cm<sup>-1</sup> for each vibrational component; the computed Franck-Condon factors of some major vibrational progressions are shown as bar diagrams above the simulated SVL emission spectrum (see text for details).

which may be recorded following a LIF study of the  $\tilde{a}-\tilde{X}$  band of SnCl<sub>2</sub>, have been simulated, and are shown in Figs. 3 and 4, respectively, with the computed FC factors of the major vibrational progressions also displayed separately as bar diagrams above the simulated spectra. (Computed FC factors of all the simulated spectra reported here are available from the authors.) The excitation lines required to produce these two SVL emissions have very close computed energies of 24 229.49 and 24 228.63 cm<sup>-1</sup>, respectively. (Note that the redshift wave number scale in each simulated SVL emission spectrum is displacement from the excitation energy, giving a direct measure of the ground state vibrational energy, as normally used by spectroscopists.) Nevertheless, the  $\tilde{a}(1,7,0)-\tilde{X}(0,0,0)$  and  $\tilde{a}(0,11,0)-\tilde{X}(0,0,0)$  vibrational components to be observed in the LIF spectrum of SnCl<sub>2</sub> have very different computed FC factors of 0.0259 and 0.9759, respectively. Recording the  $\tilde{a}(1,7,0)-\tilde{X}$  and  $\tilde{a}(0,11,0)-\tilde{X}$  SVL emissions following a LIF study of the  $\tilde{a}-\tilde{X}$  band will certainly assist spectral assignments. The vibrational structure of the  $\tilde{a}(1,7,0)-\tilde{X}$  emission is mainly due to the  $\tilde{a}(1,7,0)-\tilde{X}(1,\nu_2',0)$  progression with minor contribu-

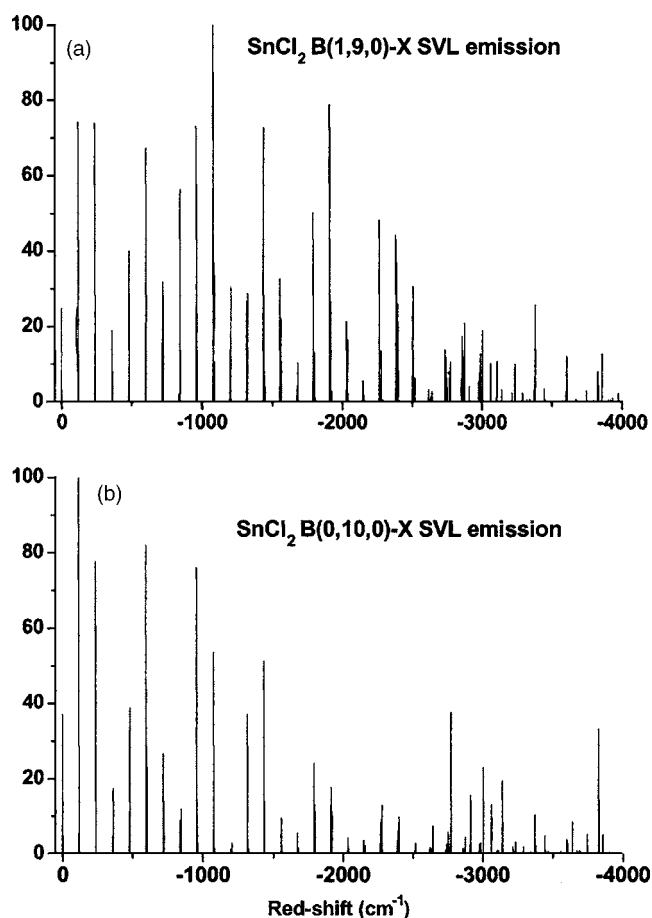


FIG. 5. Simulated SVL emission spectra of SnCl<sub>2</sub> with a FWHM of 1 cm<sup>-1</sup> for each vibrational component: (a) the  $\tilde{B}(1,9,0)-\tilde{X}$  emission resulting from an excitation energy of 31 735.34 cm<sup>-1</sup> from the  $\tilde{X}(0,0,0)$  level (top trace) and (b) the  $\tilde{B}(0,10,0)-\tilde{X}$  emission resulting from an excitation energy of 31 539.72 cm<sup>-1</sup> from the  $\tilde{X}(0,0,0)$  level (bottom trace); see text for details.

tions from the  $\tilde{a}(1,7,0)-\tilde{X}(0,\nu_2'',0)$ ,  $\tilde{a}(1,7,0)-\tilde{X}(2,\nu_2'',0)$ , and  $\tilde{a}(1,7,0)-\tilde{X}(3,\nu_2'',0)$  progressions (see bar diagrams in Fig. 3). The vibrational structure of the  $\tilde{a}(0,11,0)-\tilde{X}$  emission is mainly due to the  $\tilde{a}(0,11,0)-\tilde{X}(0,\nu_2'',0)$  progression with minor contributions from the  $\tilde{a}(0,11,0)-\tilde{X}(1,\nu_2'',0)$ ,  $\tilde{a}(0,11,0)-\tilde{X}(2,\nu_2'',0)$ , and  $\tilde{a}(0,11,0)-\tilde{X}(3,\nu_2'',0)$  progressions (see bar diagrams in Fig. 4).

The simulated  $\tilde{B}(1,9,0)-\tilde{X}(0,0,0)$  and  $\tilde{B}(0,10,0)-\tilde{X}(0,0,0)$  SVL emission spectra are shown in Fig. 5 (top and bottom traces, respectively). The excitation lines for these two SVL emissions have energies of 31 735.33 and 31 539.72 cm<sup>-1</sup>, and the vibrational components of the  $\tilde{B}(1,9,0)-\tilde{X}(0,0,0)$  and  $\tilde{B}(0,10,0)-\tilde{X}(0,0,0)$  excitations have computed FC factors of 0.1618 and 0.3988, respectively. The vibrational structure of the  $\tilde{B}(1,9,0)-\tilde{X}$  emission is mainly due to the  $\tilde{B}(1,9,0)-\tilde{X}(1,\nu_2'',0)$  and  $\tilde{B}(1,9,0)-\tilde{X}(0,\nu_2'',0)$  progressions with minor contributions from the  $\tilde{B}(1,9,0)-\tilde{X}(2,\nu_2'',0)$  and  $\tilde{B}(1,9,0)-\tilde{X}(3,\nu_2'',0)$  progressions. The vibrational structure of the  $\tilde{B}(0,10,0)-\tilde{X}$  emission is mainly due to the  $\tilde{B}(0,10,0)-\tilde{X}(0,\nu_2'',0)$  progres-

sion with minor contributions from the  $\tilde{B}(0, 10, 0)-\tilde{X}(1, \nu_2', 0)$ ,  $\tilde{B}(0, 10, 0)-\tilde{X}(2, \nu_2', 0)$ , and  $\tilde{B}(0, 10, 0)-\tilde{X}(3, \nu_2', 0)$  progressions.

## CONCLUDING REMARKS

State-of-the-art *ab initio* calculations have been carried out on low-lying singlet and triplet electronic states of SnCl<sub>2</sub>. The theoretical singlet-triplet gap of SnCl<sub>2</sub> has been estimated to be  $2.887 \pm 0.007$  eV. Computed relative electronic energies and the computed fundamental  $\nu_2'$  frequency of  $85.4 \text{ cm}^{-1}$  of the  $\tilde{a}^3B_1$  state of SnCl<sub>2</sub>, and computed FC factors for the electronic transition between the  $\tilde{a}^3B_1$  and  $\tilde{X}^1A_1$  states obtained in the present study appear to support the assignment of previously observed emission spectra<sup>52,53</sup> to the  $\tilde{a}-\tilde{X}$  band system of SnCl<sub>2</sub>. However, the best theoretical  $T_0$  value is significantly larger than the available experimental values of 2.757 (Ref. 52) and 2.759 (Ref. 53) eV. Nevertheless, our computed FC factors suggest a very weak  $\tilde{a}(0,0,0)-\tilde{X}(0,0,0)$  region of the emission band, and hence the observed band system is most likely in the vertical region. In conclusion, the best theoretical  $T_0$  value for the  $\tilde{a}^3B_1$  state of SnCl<sub>2</sub> is believed to be more reliable than the available experimental values.

It should be noted that a short research note, which reported the observation of the spectrum of Sn<sub>2</sub> (from a heated graphite hollow discharge containing tin chips) 20 years ago, concluded that the emission spectrum reported and attributed to SnCl<sub>2</sub> in Ref. 52 should actually be due to Sn<sub>2</sub>.<sup>84</sup> The aim of this work<sup>84</sup> was to draw the attention of spectroscopists to the conclusion that “the spectrum of SnCl<sub>2</sub> is still to be found.” It is surprising that no electronic spectrum, absorption, or emission of SnCl<sub>2</sub> has been recorded since, despite the fact that the He I and/or He II photoelectron spectra of SnCl<sub>2</sub> have been recorded in numerous occasions.<sup>59–63</sup> In this connection, we call for spectroscopists to record the absorption, LIF, and SVL emission spectra of SnCl<sub>2</sub> in the laboratory [such as by heating crystalline SnCl<sub>2</sub> to  $\sim 260$  °C (Ref. 62) in the throat of a nozzle in a supersonic expansion].<sup>83</sup> Simulated  $\tilde{a}-\tilde{X}$  and  $\tilde{B}-\tilde{X}$  absorption spectra of SnCl<sub>2</sub>, and also some selected  $\tilde{a}-\tilde{X}$  and  $\tilde{B}-\tilde{X}$  SVL emission spectra published in the present study should assist locating the  $\tilde{a}-\tilde{X}$  and/or  $\tilde{B}-\tilde{X}$  band systems, analyses of the observed spectra and provide fingerprint type identification of SnCl<sub>2</sub> in the gas phase, whether in a laboratory or an industrial environment of a CVD reactor.

Lastly, it should be noted that although the  $(1)^1B_1$  and  $(1)^1A_2$  states of SnCl<sub>2</sub> are calculated to be close in energy, our calculations consistently give the  $(1)^1A_2$  state to be the lowest excited singlet state of SnCl<sub>2</sub>, not the  $(1)^1B_1$  state, as normally assumed for the dihalides of the group 14 elements. Therefore, it is concluded here that the  $\tilde{A}$  state of SnCl<sub>2</sub> is the  $(1)^1A_2$  state. This conclusion is in line with the same finding from our previous study on GeCl<sub>2</sub>.<sup>38</sup> However, because of a very small equilibrium bond angle of the  $\tilde{A}^1A_2$  state (when compared with the  $\tilde{X}^1A_1$  state), a higher vertical excitation energy of the  $\tilde{A}^1A_2$  state than the  $\tilde{B}^1B_1$  state, and the most

important fact that the electronic transition between the  $\tilde{A}^1A_2$  and  $\tilde{X}^1A_1$  states is dipole forbidden, the  $(1)^1B_1-\tilde{X}^1A_1$  band and not the  $(1)^1A_2-\tilde{X}^1A_1$  band has been observed spectroscopically as the lowest energy singlet band for the dihalides of the group 14 elements (see, for example, Refs. 31, 40, 50, and 51, and references therein). Consequently, the  $(1)^1B_1$  state has been taken to be the  $\tilde{A}$  state. Nevertheless, it is noted that vibronic coupling involving the asymmetric stretching mode could lead to nonadiabatic interaction between the  $\tilde{A}^1A_2$  and  $\tilde{B}^1B_1$  states. Such nonadiabatic interaction may perturb the higher energy region of the  $\tilde{B}-\tilde{X}$  band system. Although the observed  $\tilde{A}^1B_1-\tilde{X}^1A_1$  band systems of CF<sub>2</sub>,<sup>51</sup> CCl<sub>2</sub>,<sup>50</sup> and SiCl<sub>2</sub> (Ref. 40) do not show any such perturbation, the  $\tilde{A}^1B_1-\tilde{X}^1A_1$  LIF band of GeCl<sub>2</sub> does show an abrupt change in the vibrational structure from a well resolved region to a diffuse region, which is still not fully understood.<sup>51</sup> A further investigation on the electronic energy surfaces of the  $\tilde{A}^1A_2$  and  $\tilde{B}^1B_1$  states including nonadiabatic interaction between these two states may clarify the situation.

## ACKNOWLEDGMENTS

The authors are grateful to the Research Committee of the Hong Kong Polytechnic University of HKSAR (Grant No. G-YF09) and the Research Grant Council (RGC) of the Hong Kong Special Administrative Region (HKSAR, Grant Nos. AoE/B-10/1 PolyU and PolyU 501406) for financial support. The provision of computational resources from the EPSRC (UK) National Service for Computational Chemistry Software is also acknowledged.

<sup>1</sup>G. E. Zaikov and S. M. Lomakin, *Polym. Degrad. Stab.* **54**, 223 (1996).

<sup>2</sup>G. E. Zaikov and S. M. Lomakin, *J. Appl. Polym. Sci.* **68**, 715 (1998).

<sup>3</sup>J. Jang, J. Kim, and J.-Y. Bae, *Polym. Degrad. Stab.* **90**, 508 (2005).

<sup>4</sup>D. H. Nguyen, G. Laurenczy, M. Urrutigoity, and P. Kalck, *Eur. J. Inorg. Chem.* **2005**, 4215.

<sup>5</sup>J. F. Silvain, O. Fouassier, and S. Lescaux, *J. Appl. Phys.* **96**, 4945 (2004).

<sup>6</sup>P. De, *Synlett.* **10**, 1835 (2004).

<sup>7</sup>X. H. Tan, Y. Q. Hou, C. Huang, L. Liu, and Q. X. Guo, *Tetrahedron* **60**, 6129 (2004).

<sup>8</sup>Y. J. Yang and B. J. Xiang, *Appl. Phys. A: Mater. Sci. Process.* **83**, 461 (2006).

<sup>9</sup>U. Kersen and L. Holappa, *Anal. Chim. Acta* **562**, 110 (2006).

<sup>10</sup>Z. Zainal, A. J. Ali, A. Kassim, and M. Z. Hussein, *Sol. Energy Mater. Sol. Cells* **79**, 125 (2003).

<sup>11</sup>J. P. Ge, J. Wang, H. X. Zhang, X. Wang, Q. Peng, and Y. D. Li, *Sens. Actuators B* **113**, 937 (2006).

<sup>12</sup>V. Hopfe, D. W. Sheel, C. I. M. A. Spee, R. Tell, P. Martin, A. Beil, M. Pemble, R. Weiss, U. Vogt, and W. Graehlert, *Thin Solid Films* **442**, 60 (2003).

<sup>13</sup>K. Takahashi, A. Kunz, D. Woiki, and P. Roth, *J. Phys. Chem. A* **104**, 5246 (2000).

<sup>14</sup>V. Hopfe, D. W. Sheel, W. Graehlert, and O. Throl, *Surf. Coat. Technol.* **142**, 142 (2001).

<sup>15</sup>See, for example, N. Bulcourt, J.-P. Booth, E. A. Hudson, J. Luque, D. K. W. Mok, E. P. F. Lee, F.-t. Chau, and J. M. Dyke, *J. Chem. Phys.* **120**, 9499 (2004) and reference therein.

<sup>16</sup>M. Nakamura, M. Hori, T. Goto, M. Ito, and N. Nishii, *J. Appl. Phys.* **90**, 580 (2001).

<sup>17</sup>G. A. Hebner, *J. Appl. Phys.* **89**, 900 (2001).

<sup>18</sup>J. P. Booth, *Plasma Sources Sci. Technol.* **8**, 249 (1999).

<sup>19</sup>B. K. McMillin and M. R. Zachariah, *J. Vac. Sci. Technol. A* **15**, 230 (1997).

- <sup>20</sup>C. Suzuki, K. Sasaki, and K. Kadota, *J. Vac. Sci. Technol. A* **16**, 2222 (1998).
- <sup>21</sup>G. Cunge and J. P. Booth, *J. Appl. Phys.* **85**, 3952 (1999).
- <sup>22</sup>B. A. Cruden, K. K. Gleason, and H. H. Sawin, *J. Appl. Phys.* **89**, 915 (2001).
- <sup>23</sup>H. Kim and F. L. Terry, Jr., *Proc. SPIE* **136**, 3642 (1999).
- <sup>24</sup>R. J. H. Klein-Douwel, J. J. Schermer, and J. J. ter Meulen, *Diamond Relat. Mater.* **7**, 1118 (1998).
- <sup>25</sup>A. G. Lowe, A. T. Hartlieb, J. Brand, B. Atakan, and K. Kohse-Hoinghaus, *Combust. Flame* **118**, 37 (1999).
- <sup>26</sup>A. Goossens, W. F. A. Besling, and J. Schoonman, *J. Phys. IV* **9**, 519 (1999).
- <sup>27</sup>D. P. Liu, I. T. Martin, and E. R. Fisher, *Chem. Phys. Lett.* **430**, 113 (2006).
- <sup>28</sup>H. Ito, K. Oda, and H. Saitoh, *Thin Solid Films* **506**, 715 (2006).
- <sup>29</sup>A. Hibi, H. Tonegawa, K. Tonokura, K. Satake, H. Sakamoto, and M. Koshi, *Surf. Coat. Technol.* **200**, 3117 (2006).
- <sup>30</sup>H.-J. Hsu, W.-Z. Chang, and B.-C. Chang, *Phys. Chem. Chem. Phys.* **7**, 2468 (2005).
- <sup>31</sup>Y.-S. Lin, C.-C. Chen, and B.-C. Chang, *J. Chem. Phys.* **124**, 224322 (2006).
- <sup>32</sup>H. Fan, C. Mukarakate, M. Deselnicu, C. Tao, and S. A. Reid, *J. Chem. Phys.* **123**, 014314 (2005).
- <sup>33</sup>B. S. Tackett and D. J. Clouthier, *J. Chem. Phys.* **123**, 144304 (2005).
- <sup>34</sup>B. S. Tackett, S.-G. He, C. J. Evans, D. J. Clouthier, and R. H. Judge, *J. Chem. Phys.* **119**, 2037 (2003).
- <sup>35</sup>R. de Nalda, A. Mavromanolakis, S. Couris, and M. Castillejo, *Chem. Phys. Lett.* **316**, 449 (2000).
- <sup>36</sup>D. A. Hostutler, D. J. Clouthier, and R. H. Judge, *J. Chem. Phys.* **114**, 10728 (2001).
- <sup>37</sup>J. Lei, A. Teslja, B. Nizamov, and P. J. Dagdigian, *J. Phys. Chem. A* **105**, 7828 (2001).
- <sup>38</sup>D. K. W. Mok, F.-t. Chau, E. P. F. Lee, and J. M. Dyke, *ChemPhysChem* **6**, 719 (2005).
- <sup>39</sup>E. P. F. Lee, D. K. W. Mok, F.-t. Chau, and J. M. Dyke, *J. Chem. Phys.* **121**, 2962 (2004).
- <sup>40</sup>F.-t. Chau, D. C. Wang, E. P. F. Lee, and J. M. Dyke, *J. Phys. Chem. A* **103**, 4925 (1999).
- <sup>41</sup>E. P. F. Lee, D. K. W. Mok, J. M. Dyke, and F.-t. Chau, *J. Phys. Chem. A* **106**, 10130 (2002).
- <sup>42</sup>D. K. W. Mok, E. P. F. Lee, F.-t. Chau, and J. M. Dyke, *J. Chem. Phys.* **120**, 1292 (2004).
- <sup>43</sup>F.-t. Chau, D. K. W. Mok, E. P. F. Lee, and J. M. Dyke, *J. Chem. Phys.* **121**, 1810 (2004).
- <sup>44</sup>D. K. W. Mok, E. P. F. Lee, F.-t. Chau, and J. M. Dyke, *J. Comput. Chem.* **22**, 1896 (2001).
- <sup>45</sup>D. K. W. Mok, E. P. F. Lee, F.-t. Chau, D. C. Wang, and J. M. Dyke, *J. Chem. Phys.* **113**, 5791 (2000).
- <sup>46</sup>D. C. Wang, F.-t. Chau, D. K. W. Mok, E. P. F. Lee, L. Beeching, J. S. Ogden, and J. M. Dyke, *J. Chem. Phys.* **114**, 10682 (2001).
- <sup>47</sup>D. K. W. Mok, F.-t. Chau, E. P. F. Lee, and J. M. Dyke, *J. Chem. Phys.* **125**, 104303 (2006).
- <sup>48</sup>E. P. F. Lee, D. K. W. Mok, F.-t. Chau, and J. M. Dyke, *J. Chem. Phys.* **125**, 104304 (2006).
- <sup>49</sup>F.-t. Chau, D. K. W. Mok, E. P. F. Lee, and J. M. Dyke, *ChemPhysChem* **6**, 2037 (2005).
- <sup>50</sup>J. M. Dyke, E. P. F. Lee, D. K. W. Mok, and F.-t. Chau, *ChemPhysChem* **6**, 2046 (2005).
- <sup>51</sup>F.-t. Chau, J. M. Dyke, E. P. F. Lee, and D. K. W. Mok, *J. Chem. Phys.* **115**, 5816 (2001).
- <sup>52</sup>R. K. Asundi, M. Karim, and R. Samuel, *Proc. Phys. Soc. London* **50**, 581 (1938).
- <sup>53</sup>D. Naegli and H. B. Palmer, *J. Mol. Spectrosc.* **21**, 325 (1966).
- <sup>54</sup>I. R. Beattie and R. O. Perry, *J. Chem. Soc. A* **1970**, 2429.
- <sup>55</sup>A. Y. Nasarenko, V. P. Spiridonov, B. S. Butayev, and E. Z. Zasorin, *J. Mol. Struct.: THEOCHEM* **119**, 263 (1985).
- <sup>56</sup>A. G. Gershikov, E. Z. Zasorin, A. V. Demidov, and V. P. Spiridonov, *Zh. Strukt. Khim.* **27**, 36 (1986).
- <sup>57</sup>K. V. Ermakov, B. S. Butayev, and V. P. Spiridonov, *J. Mol. Struct.* **248**, 143 (1991).
- <sup>58</sup>M. Fields, R. Devonshire, H. G. M. Edwards, and V. Fawcett, *Spectrochim. Acta, Part A* **51**, 2249 (1995).
- <sup>59</sup>D. H. Harris, M. F. Lappert, J. B. Pedley, and G. J. Sharp, *J. Chem. Soc. Dalton Trans.* **1976**, 945.
- <sup>60</sup>S. Evans and A. F. Orchard, *J. Electron Spectrosc. Relat. Phenom.* **6**, 207 (1975).
- <sup>61</sup>I. Novak and A. W. Potts, *J. Electron Spectrosc. Relat. Phenom.* **33**, 1 (1984).
- <sup>62</sup>C. Cauletti, M. de Simone, and S. Stranges, *J. Electron Spectrosc. Relat. Phenom.* **57**, R1 (1991).
- <sup>63</sup>S. Stranges, M. Y. Adam, C. Cauletti, M. de Simone, C. Furlani, M. N. Piancastelli, P. Declava, and A. Lisini, *J. Chem. Phys.* **97**, 4764 (1992).
- <sup>64</sup>J. M. Ricart, J. Rubio, and F. Illas, *Chem. Phys. Lett.* **123**, 528 (1986).
- <sup>65</sup>M. Benavidesgarcia and K. Balasubramanian, *J. Chem. Phys.* **100**, 2821 (1994).
- <sup>66</sup>E. Sicilia, M. Toscano, T. Mineva, and N. Russo, *Int. J. Quantum Chem.* **61**, 571 (1997).
- <sup>67</sup>A. Szabados and M. Hargittai, *J. Phys. Chem. A* **107**, 4314 (2003).
- <sup>68</sup>I. M. B. Nielsen, C. L. Janssen, and M. D. Allendorf, *J. Phys. Chem. A* **107**, 5122 (2003).
- <sup>69</sup>J. B. Levy, G. Jancso, and M. Hargittai, *J. Phys. Chem. A* **107**, 10450 (2003).
- <sup>70</sup>S. Escalante, R. Vargas, and A. Vela, *J. Phys. Chem. A* **103**, 5590 (1999).
- <sup>71</sup>K. Hilpert, S. Roszak, J. Saloni, M. Miller, P. Lipkowski, and J. Leszczynski, *J. Phys. Chem. A* **109**, 1286 (2005).
- <sup>72</sup>L.-C. Li, P. Deng, Y.-Q. Zhu, D. Zha, A. N.-M. Tian, M.-H. Xu, and N.-B. Wong, *Int. J. Quantum Chem.* **104**, 367 (2005).
- <sup>73</sup>H. G. Yu and S. J. Sears, *J. Chem. Phys.* **125**, 114316 (2006).
- <sup>74</sup>P. J. Knowles, C. Hampel, and H.-J. Werner, *J. Chem. Phys.* **99**, 5219 (1993); **112**, 3106(E) (2000).
- <sup>75</sup>H.-J. Werner and P. J. Knowles, *J. Chem. Phys.* **89**, 5803 (1988).
- <sup>76</sup>B. Metz, H. Stoll, and M. Dolg, *J. Chem. Phys.* **113**, 2563 (2000).
- <sup>77</sup>For pseudopotentials of the Stuttgart/Cologne group, see the website: <http://www.theochem.uni-stuttgart.de/pseudopotentials/index.en.html>
- <sup>78</sup>K. A. Peterson, *J. Chem. Phys.* **119**, 11099 (2003).
- <sup>79</sup>(<http://www.emsl.pnl.gov/forms/basisform.html>): The Extensible Computational Chemistry Environment Basis Set Database, Version 02/25/04, as developed and distributed by the Molecular Science Computing Facility, Environmental and Molecular Sciences Laboratory which is part of the Pacific Northwest Laboratory, P.O. Box 999, Richland, Washington 99352, and funded by the U.S. Department of Energy. The Pacific Northwest Laboratory is a multiprogram laboratory operated by Battelle Memorial Institute for the U.S. Department of Energy under Contract No. DE-AC06-76RLO 1830. Contact Karen Schuchardt for further information.
- <sup>80</sup>T. H. Dunning, Jr., K. A. Peterson, and A. K. Wilson, *J. Chem. Phys.* **114**, 9244 (2001).
- <sup>81</sup>H.-J. Werner, P. J. Knowles, M. Schütz *et al.*, MOLPRO is a package of *ab initio* programs.
- <sup>82</sup>J. K. G. Watson, *Mol. Phys.* **15**, 479 (1968).
- <sup>83</sup>J. Karolczak, Q. Zhuo, D. J. Clouthier, W. M. Davis, and J. D. Goddard, *J. Chem. Phys.* **98**, 60 (1993).
- <sup>84</sup>I. Dubois, *J. Mol. Spectrosc.* **124**, 494 (1987).
- <sup>85</sup>T. Fjeldberg, A. Hanland, B. E. R. Schilling, M. F. Lappert, and A. J. Thorne, *J. Chem. Soc. Dalton Trans.* **1986**, 1551.